Far Infrared Spectra of Silicate Minerals

for Use in Remote Sensing of Lunar and Planetary Surfaces

PREPARED FOR NASA
MARSHALL SPACE FLIGHT CENTER

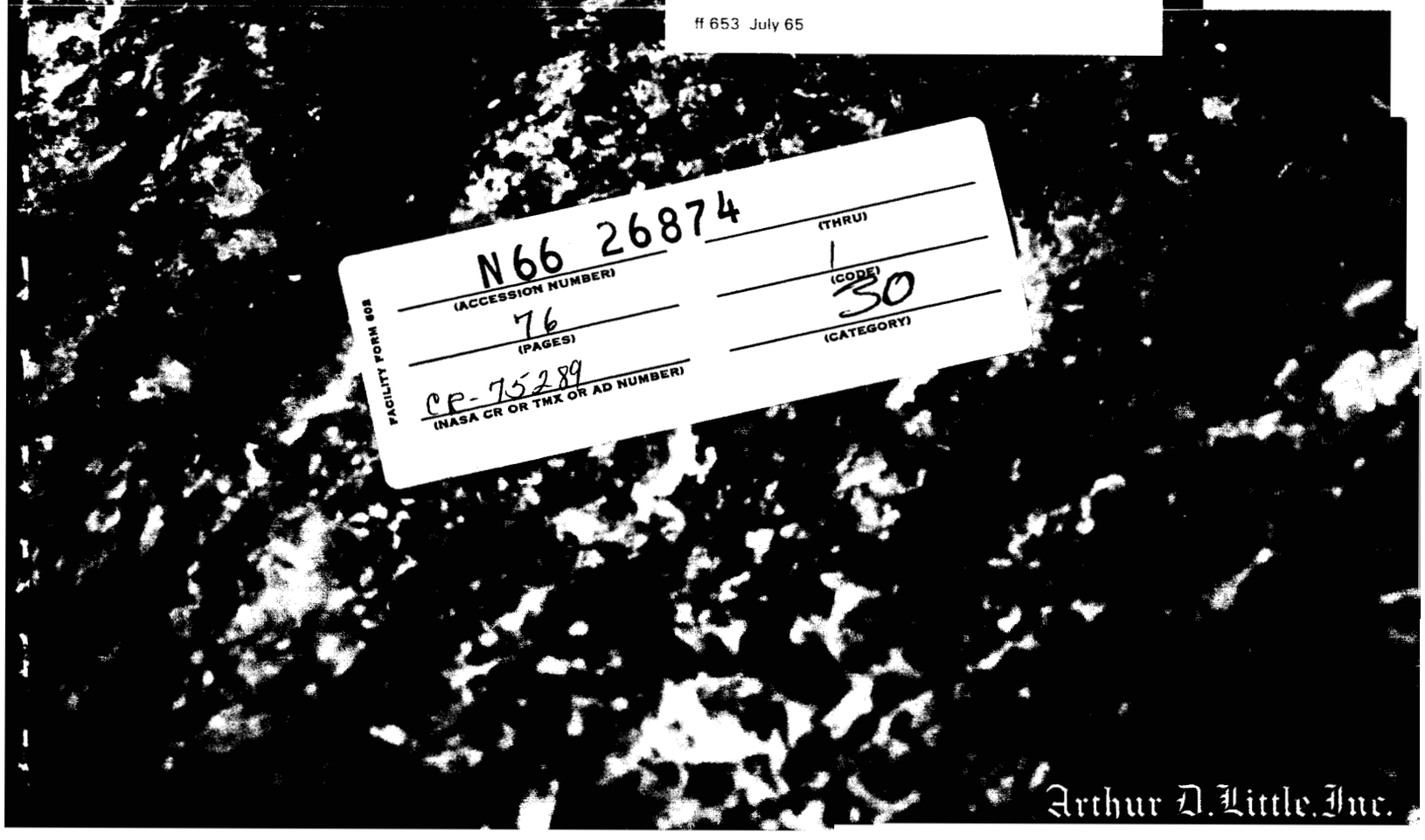

Arthur D. Little, Inc.

FAR INFRARED SPECTRA OF SILICATE MINERALS FOR USE IN REMOTE SENSING OF LUNAR AND PLANETARY SURFACES

by

James R. Aronson, Alfred G. Emslie, Ronald V. Allen,
and Hugh G. McLinden

FINAL REPORT
April 1965 - April 1966
Under Contract No. NAS 8-20122

Prepared for

George C. Marshall Space Flight Center
National Aeronautics and Space Administration
Huntsville, Alabama

Prepared by

Arthur D. Little, Inc.
15 Acorn Park
Cambridge, Massachusetts

April 15, 1966
C-67323

TABLE OF CONTENTS

LIST OF TABLES AND FIGURES

LIST OF TABLES AND FIGURES (continued)

ABSTRACT

26874

This report is concerned with the results of an experimental and theoretical investigation of the far infrared spectra of silicate minerals for use in remote sensing of the composition of lunar or planetary surfaces. The subject matter consists of

1) an examination of the spectral information that may be obtained from silicate minerals in the far infrared region;

2) a study of the effects of the state of surface aggregation, especially for fine particulate surfaces, on the information content of such spectra;

3) considerations of the ways in which the spectra of composite samples may be understood in terms of the spectra of their components, and

4) a brief description of the instrumental considerations that would be involved in utilizing these results on a space mission.

FAR INFRARED SPECTRA OF SILICATE MINERALS FOR USE IN REMOTE SENSING OF LUNAR AND PLANETARY SURFACES

I. INTRODUCTION

This report details the results and conclusions of our study of mineral spectroscopy in the far infrared region of the spectrum. Our studies have been concentrated in the 15-200μ (667-50 cm^{-1}) region. The objectives of this work were to examine the problems and ascertain the feasibility of remote sensing of the composition of the Moon (or tenuous atmosphere planets, such as Mars) and evaluate the importance of the far infrared spectral region to this end. We initiated our studies in this area under a previous contract[1] to which we will refer repeatedly, but we intend to utilize some of the results of that work in this report so as to obviate the need for continual reference to the earlier report.

The subject matter has naturally devolved into a series of smaller problem areas that we have pursued concurrently to some degree. They are:

1. The degree of useful mineral spectroscopic information present in the far infrared and its characteristic similarities and differences from that obtainable in the near and middle infrared regions.

2. The effects of departures from optically smooth surfaces (principally to fine particulate surfaces) on the information content of spectra in general.

3. The nature of the ways in which the spectra of composite samples may be derived from the spectra of individual minerals and the resulting implications for disentangling composite spectra in practical cases.

In addition, our work on these problems stimulated Arthur D. Little, Inc., to consider the precise kind of equipment that would be most useful in carrying out the actual exploration and mapping of lunar or planetary surface composition. Our judgments on this subject were detailed in a proposal[2], entitled "Mapping of the Composition of the Surface and Atmosphere of Mars by an Orbiting Broadband Infrared Interferometer," intended for the Voyager Mission. We will discuss each of these subjects in some detail in the body of this report.

For many years the field of mineral infrared spectroscopy has received considerable attention. Lyon has compiled a comprehensive bibliography[3] on this subject in the course of carrying out an extensive program himself.[4,5] Most investigators have concentrated their efforts in the near and middle infrared regions for which commercial instruments have long been available. The far infrared region (i.e., beyond $\sim 25\mu$) in this as in other areas of spectroscopic research has been almost totally neglected. The reason for the neglect is simply the difficulties involved in working in this inherently low signal region of the spectrum. Most of these difficulties[6,7] relate to the lack of good sources for the region. Despite this problem, general instrumental improvements in recent years have greatly increased the amount of far infrared research taking place.[8]. In addition, lasers have now been developed for a number of discrete wavelengths in the region.[9] As this report will show, we feel that the large amount of useful spectral information in this region makes it very important to include it in plans for remote sensing of lunar and planetary surfaces.

While the far infrared spectra to be obtained in remote sensing applications from lunar or planetary surfaces will be self emission spectra, we have carried out most of our work utilizing reflection techniques. The reason for this is the comparative simplicity of the reflection method with available laboratory instruments due to the low power available in emission from cool samples. The basic experimental techniques have been discussed in a prior report.[7]

II. MINERAL SPECTROSCOPY IN THE FAR INFRARED

The far infrared region has proved to be exceedingly rich in spectral information for silicate minerals. This result is not surprising as even the highest frequency fundamentals, the antisymmetric silicon-oxygen stretching vibrations, in most silicates occur between 800 and 1200 cm^{-1}. All other fundamentals have lower force constants and hence lower frequencies. In addition, difference bands, lattice vibrations and their combinations with internal vibrations would be expected to appear in this low frequency region.

The nature of the spectral information about silicate minerals that occurs in the far infrared region is similar to that in the higher frequency region, also being due to atomic group vibrations. Such data are very useful in supplementing middle infrared data, as identification of components of complex mixtures by their spectral features is greatly aided by an increase in the number of features observed. In addition, however, there are important differences between the spectra observed in the far infrared and those in the middle infrared, and these are particularly useful in precise mineral identification.[10] These differences result in part from the greater amount of coupling between small atomic-group vibrations in the low frequency region. This coupling results in vibrations from larger aggregates and hence spectra that are more characteristic of specific minerals. The spectra may therefore be used in a finger-print sense.

At the conclusion of our previous work,[1] we pointed out the significant differences that exist in the far infrared reflection spectra of a number of silicate minerals of different structural types. In order to clarify the spectral-structure relationships, we felt that an increased number of minerals needed to be examined. We felt particular emphasis should be put on the study of spectral variations within homologous series.

A. THE OLIVINES

The first series we chose to pursue is that of the olivines, which runs from fayalite (Fe_2SiO_4) to forsterite (Mg_2SiO_4), but also contains a number of possible impurity constituents. Two samples at the forsterite end of this series have been run to go along with the fayalite spectrum of our previous work. They are a 70:30 Fo:Fa mineral obtained from Wards Natural Science Establishment and a "pure" forsterite synthesized in our laboratories. The spectra are shown in Figure 1. The 70:30 Fo:Fa olivine is a close approximation to the olivine present in the Forest City chondrite (See Section IV). The spectrum of "pure" forsterite as prepared in our laboratories is also shown in Figure 1. This material was prepared by reacting $Mg(NO_3)_2 \cdot 6H_2O$ and $Si(OC_2H_5)_4$ in anhydrous methanol. A clear liquid was produced which gelled on standing. The product was heated to remove volatile components and fired at 1600°C for 12 hours. Well crystallized "pure" Mg_2SiO_4 was identified by X-ray diffraction. We are including a slightly modified version of our original curve for fayalite in this figure. It resulted from a careful reexamination of the raw data.

The method of studying spectral variations in homologous series by preparing known isomorphic compounds has been elucidated in a recent series of papers[10,11] by Tarte. He has applied this method to transmission spectra of olivines to frequencies as low as 280 cm^{-1} (36μ). This study indicates that from 1000 cm^{-1} to 450 cm^{-1} the olivine structure is characterized by a fairly specific band pattern due to the SiO_4 tetrahedra. From 450 cm^{-1} to 280 cm^{-1}, Tarte finds the spectrum to be more influenced by the nature of the cations present. Thus it is easy to understand the large spectral variations in the low frequency region for this series when compared to the relatively small variations in the middle infrared.[4]

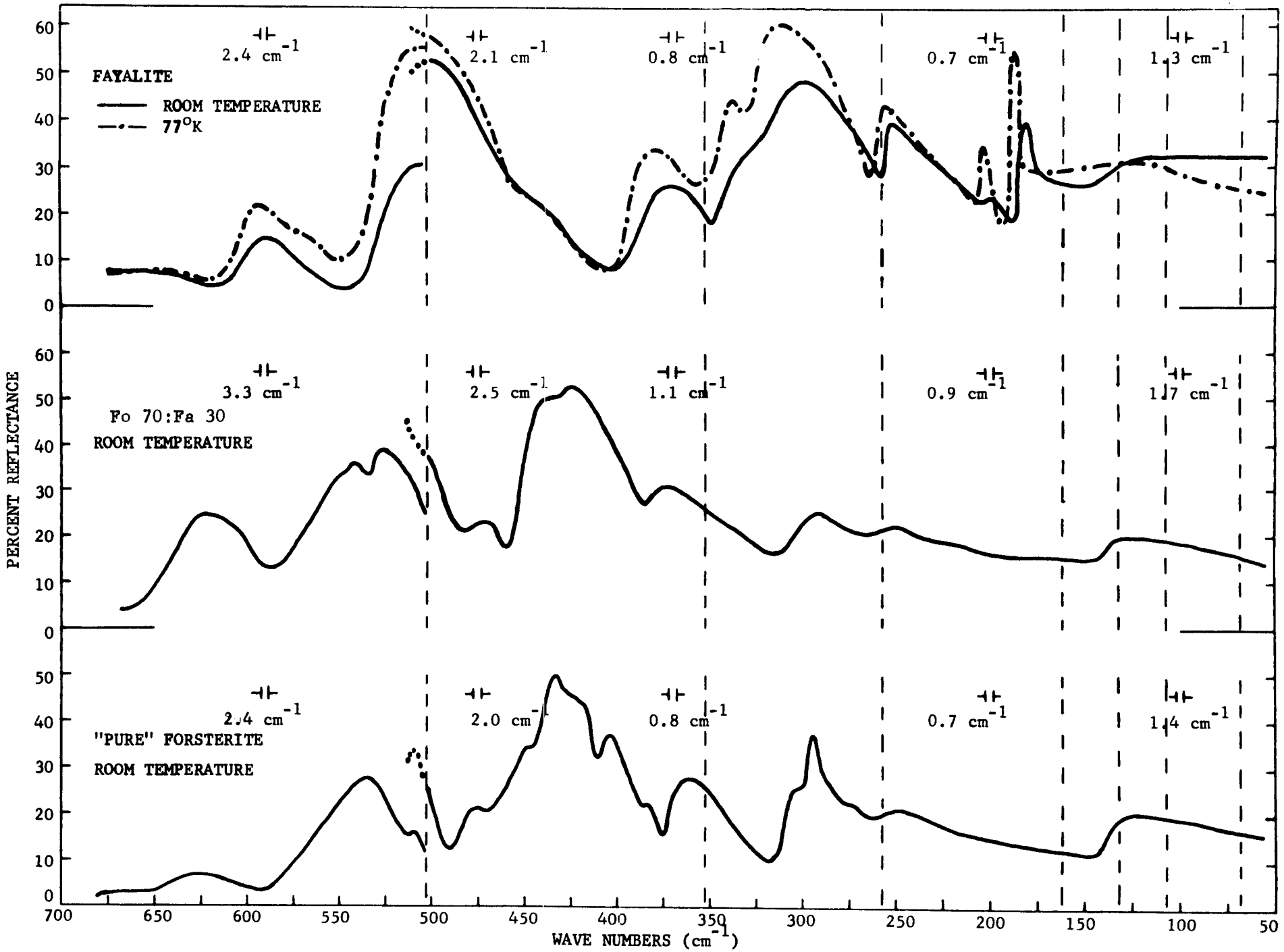

FIGURE 1. FAR INFRARED REFLECTANCE OF OLIVINES

B. THE PLAGIOCLASE FELDSPARS

In Figure 2, we show the far infrared spectra of two plagioclase feldspar minerals, albite and oligoclase. These two minerals are members of another homologous series and are close in chemical composition (albite refers to a compositional range from Ab, the "pure" mineral $NaAlSi_3O_8$, to $Ab_{90}An_{10}$ where An represents the other end member of this series, anorthite, $CaAl_2Si_2O_8$; oligoclase refers to the range $Ab_{90}An_{10}$ to $Ab_{70}An_{30}$). Here the point that orientation-polarization effects can be so great with crystal samples as to require that different orientations be considered as different minerals is well demonstrated.

It should be noted that the sample of albite used to obtain the upper spectrum was oriented so that the radiation impinged on the (001) face, and the (100) cleavage is approximately perpendicular to the plane of incidence. The (001) cleavage exposes the twin striations of plagioclase feldspars and the spectrum thus contains information from two orientations. The twinned crystals are only offset by a few degrees however so that the orientation is essentially that shown in Figure 2. As such twinning is almost universal in feldspars, exposure of this cleavage plane is very common.

A detailed examination of Figure 2 shows that the differences between two such similar minerals as similarly oriented albite and oligoclase are observable if sufficient spectral range is involved, and spectral intensities and shapes are considered as well as band frequencies. Some of the absolute intensity differences may be ascribed to difference in polish of the respective surfaces, but the relative intensities are more significant. Comparison of the two orientations of albite is interesting both from the point of view of orientation invariant features (e.g., the "albite" band near 90 cm^{-1} and perhaps the 330 cm^{-1} feature) and the drastic changes in the remainder of the spectrum. These are the types of observations necessary to assign different bands to their vibrational origins, but of secondary interest if one is dealing with

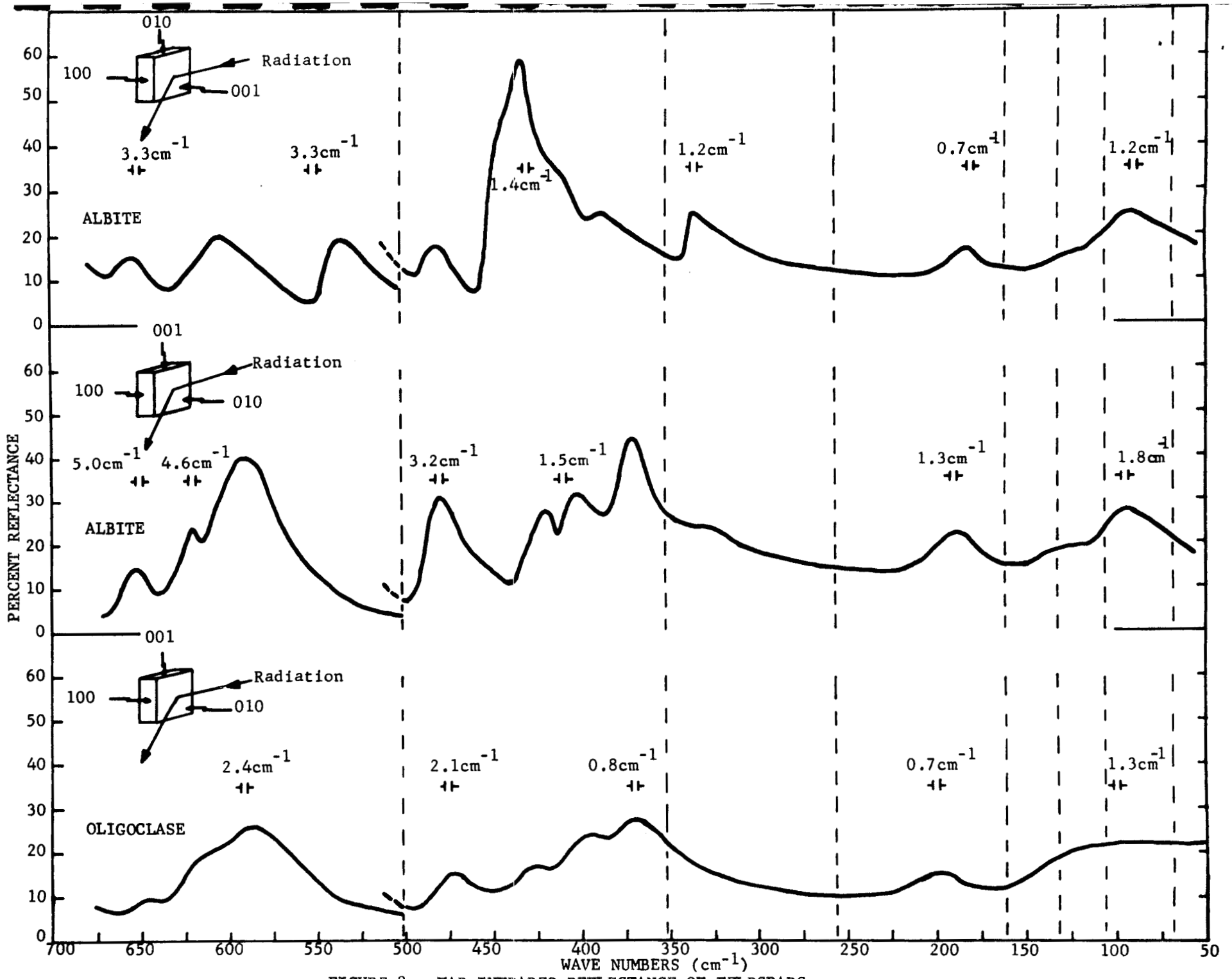

FIGURE 2. FAR INFRARED REFLECTANCE OF FELDSPARS

"randomized" samples in remote sensing applications. For the latter case randomly oriented samples are preferable to oriented crystals if one can assume no preferred orientation in natural environments.

C. SERPENTINE

We have also run serpentine, $Mg_6Si_4O_{10}(OH)_8$, a layer structure orthorhombic mineral. The spectrum shown in Figure 3 was run on a massive polycrystalline sample of this layer lattice silicate. It bears a striking resemblance, in the 250-680 cm^{-1} region, to data obtained by Hunt[12] except that we appear to have sufficiently greater resolution to clearly split the large band near 480 cm^{-1} into three components at 435 cm^{-1}, 480 cm^{-1}, and 510 cm^{-1}. These features can be observed in Hunt's spectrum though incompletely resolved.

D. HORNBLENDE

The spectrum of hornblende, an amphibole with a double chain structure, is shown in Figure 4. The single crystal was oriented so that radiation was reflected off the (001) face. The name hornblende includes a series of compositions with varying cation substitutions. A general formula is $X_{2-3}Y_{5-7}Z_8O_{22}(O,OH,F)_2$, where X can be Ca, Na; Y can be Mg, Fe, Al; and Z can be Al, Si. The composition of our sample is given in Table I.

E. ENSTATITE

In Figure 5 we have reproduced the spectra of enstatite from our previous report.[1] This mineral is orthorhombic but has a tetrahedral single chain structure. It is part of an isomorphous series, being the magnesium-rich end (FeO < 13%) of the enstatite-ferrosilite ($Mg_2Si_2O_6$-$MgFeSi_2O_6$-$Fe_2Si_2O_6$) series. Although not indicated by the formula, aluminum is often present in this series. The description accompanying the sample indicated that the enstatite was altering to

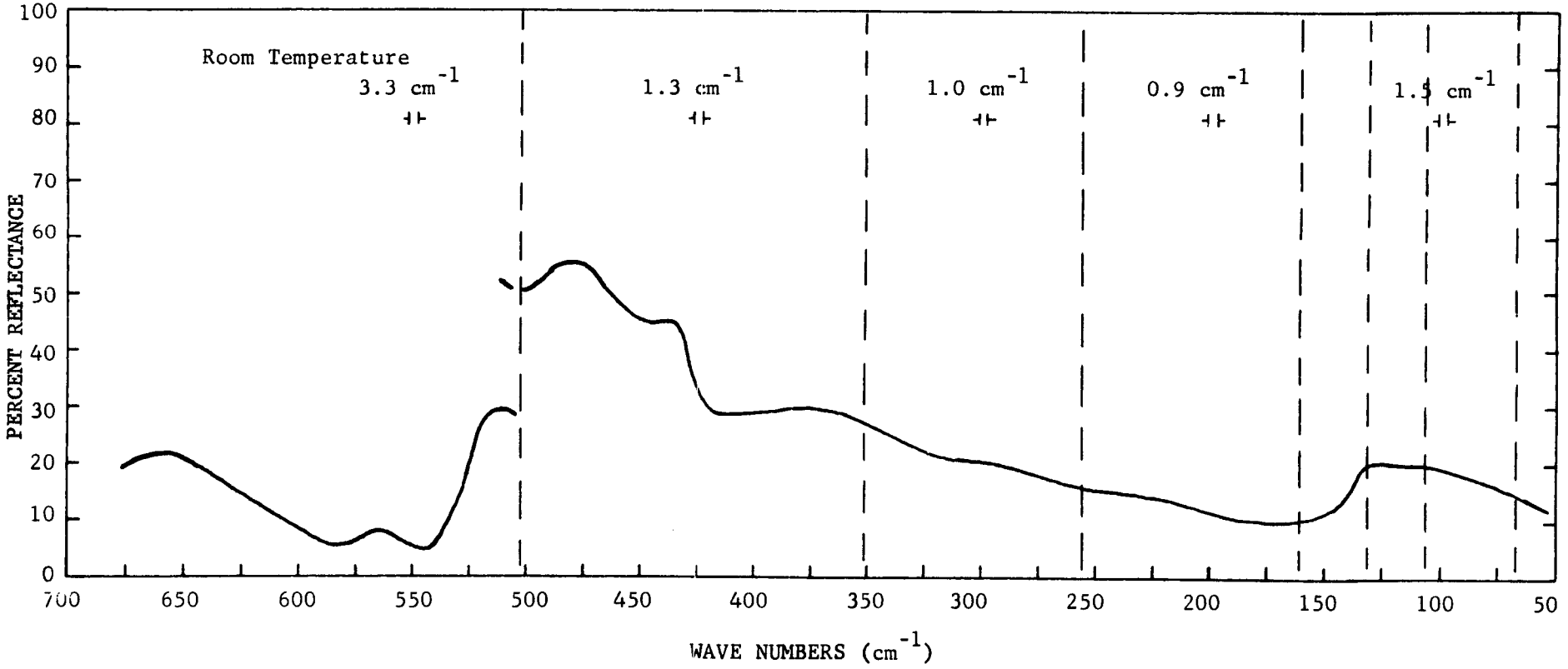

FIGURE 3. FAR INFRARED REFLECTANCE OF SERPENTINE

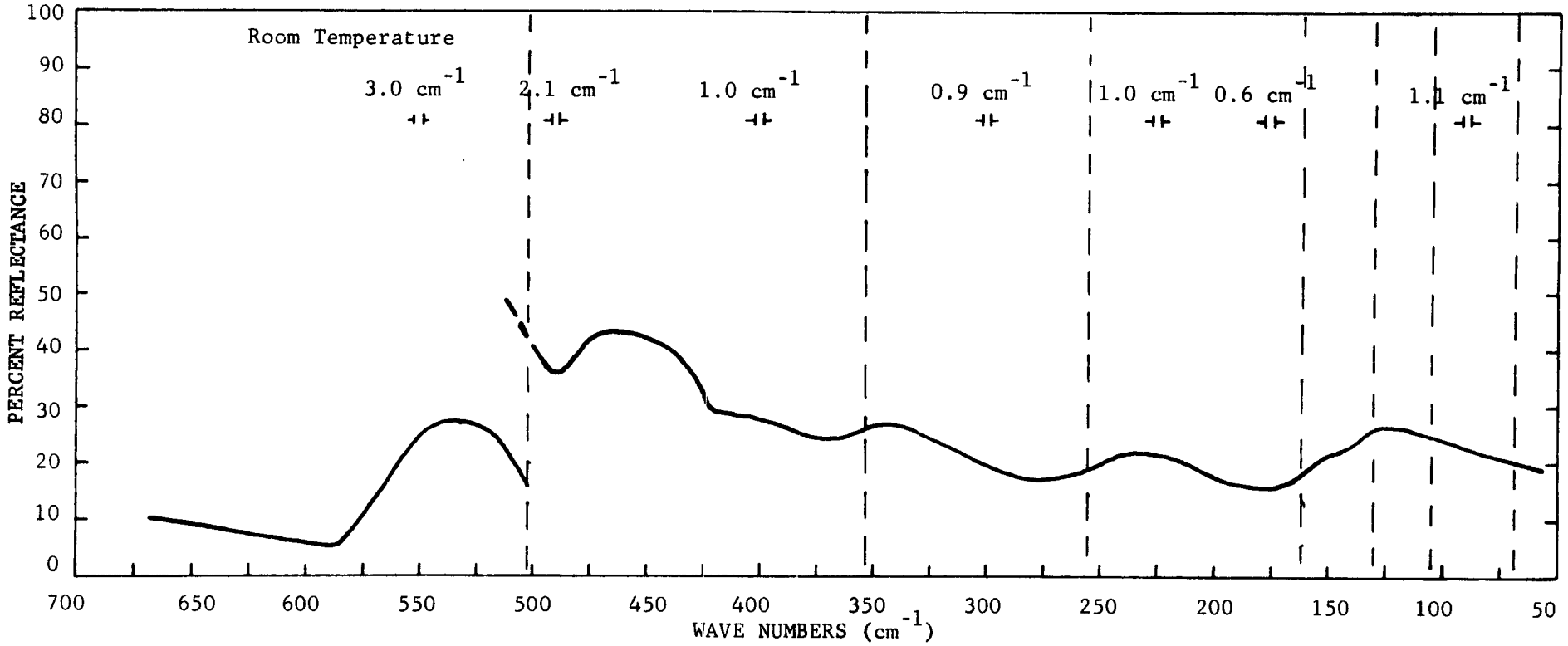

FIGURE 4. FAR INFRARED REFLECTANCE OF HORNBLENDE

TABLE I

MINERAL DATA

	MINERAL (a)	ORIGIN	COMPOSITION SiO_2	Al_2O_3	Fe_2O_3	CaO	MgO	Na_2O	FeS	CO_2	IGN. LOSS	TOTAL	CRYSTAL FACE STUDIED	POWDER SIZE MAXIMUM	POWDER SIZE MOST PARTICLES
1	Albite	Bancroft Ontario	71.5	22.6	---	1.76	---	7.30	---	---	1.10	104.26	(010)(001)		
2	Oligoclase	Mitchell Co. N. Carolina	69.4	24.0	---	3.28	---	4.85	---	---	---	101.43	(010)		
3	Hornblende	Kragero Norway	53.5	12.4	20.0	6.72	8.95	2.37	---	---	.50	104.44	(001)		
4	Enstatite	Norway	52.84	2.45	12.40	---	30.75	---	---	---	---	98.04	(100)		
5	Fayalite	Rockport Mass.	27.9	1.0	70.8	---	---	---	---	---	---	99.7	Polycrystal-line	2.6	0-1
6	Forsterite Fa_{70} Fa_{30}	Ontario	36.42	12.22	13.15	2.2	33.89	---	---	2.08	---	99.96	Polycrystal-line		
7	Forsterite synth. (c)	ADL	---	---	---	---	---	---	---	---	---		Polycrystal-line		
8	Serpentine (b)	Proctor Vermont	51.7	3.98	---	---	23.9	---	---	---	12.06	91.64	Polycrystal-line		
9	Quartz (d)		---	---	---	---	---	---	---	---	---	---		8.0	1.6-5
10	Troilite (e)	Xiquipilco Mexico	---	---	---	---	---	---	95.76	---	---	---	Polycrystal-line		
11	Andesine Pigeonite	Virginia	---	---	---	---	---	---	---	---	---	---	Polycrystal-line		
12	Chondrite	Forest City Iowa	---	---	---	---	---	---	---	---	---	---	Polycrystal-line		

TABLE I (continued)

(a) Samples 1, 2, 3, and 8 were analyzed by spectrographic methods. Individual values are accurate to within 2%.

(b) No quantitative determination for iron was made on the serpentine; however, iron as oxide is present in the 5-10% range.

(c) This sample was analyzed by X-ray diffraction. No peaks other than those for Mg_2SiO_4 we observed.

(d) Sample analyzed by X-ray diffraction only.

(e) Sample analyzed for Fe and S only.

(f) Feldspar shown to be andesine by X-ray diffraction index of refraction and extinction measurements.

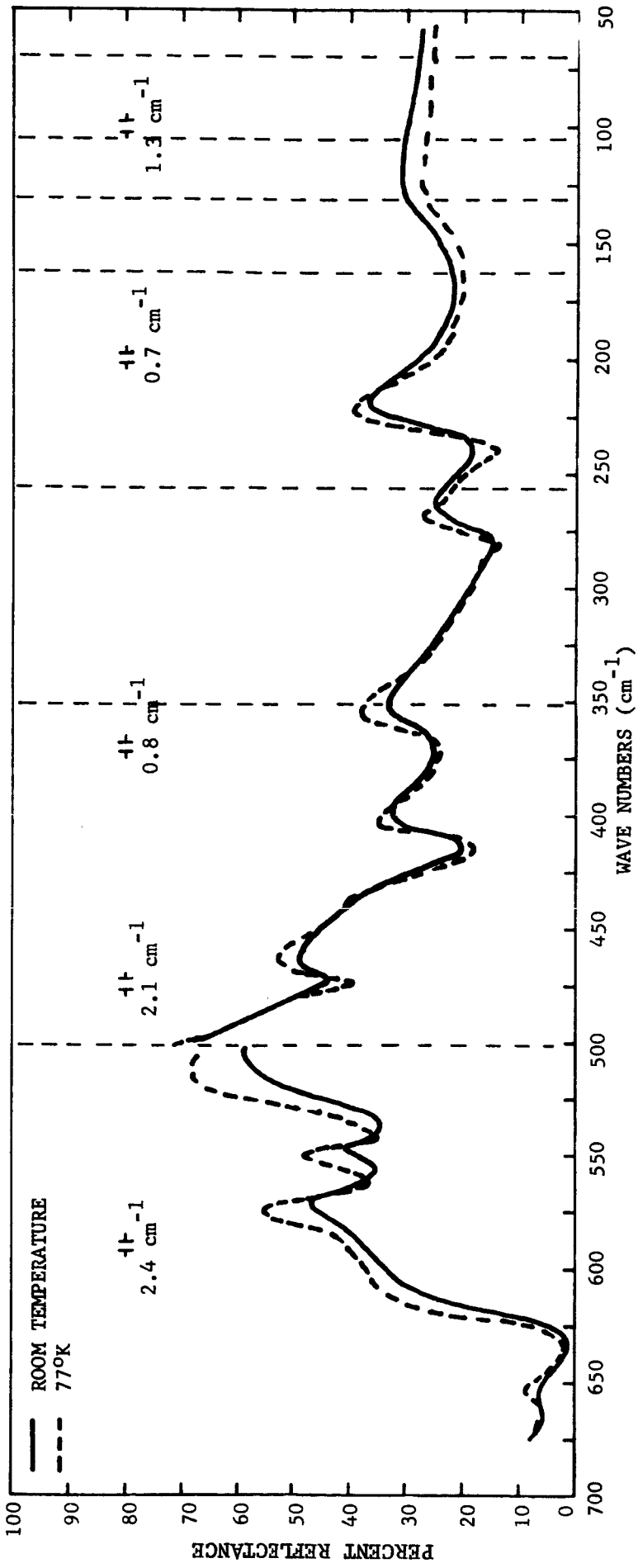

FIGURE 5. FAR INFRARED REFLECTANCE OF ENSTATITE

serpentine. Ignition of the sample at 1000°C for one hour showed a water loss, indicating approximately 7.9% serpentine by weight. Our measurements were made on the (100) face of this crystal.

F. MISCELLANEOUS COMPONENTS OF THE FOREST CITY CHONDRITE

A number of our samples were run in order to compare the spectra of individual samples and that of a composite (the Forest City Chondrite). This will be discussed in a later section.

Among these we have run the spectrum of a composite sample containing a feldspar and pigeonite. The feldspar composition is close to $Ab_{52}An_{48}$ which is an andesine (i.e., $Ab_{70}An_{30}$ to $Ab_{50}An_{50}$). It was necessary to run this sample as we were unable to obtain a sufficiently large sample of pigeonite having a composition close to that reported as being present in the Forest City Chondrite.[1]

The feldspar in this rock was determined to be Ab_{52} by measurement of the extinction angle of many particles. The index of refraction was also measured and the results for the (001) face give n between 1.560 and 1.551, thus indicating $Ab_{52}An_{48}$ as the composition of the feldspar. These results are believed accurate to within 2%. X-ray analysis of the sample indicates the feldspar to be andesine. The pyroxene fraction contains iron and has a diffraction pattern close to that of diopside. Hence it is a good approximation to the pigeonite of the Forest City Chondrite. We calculate that the composite feldspar-pigeonite sample has a composition of 65 ± 5% pigeonite and 35 ∓ 5% feldspar on the face we are examining. The estimation was carried out by making planimeter measurements on a photograph of the sample face studied. It is shown in Figure 6 along with the spectrum obtained.

In Figure 7 is shown the rather uninteresting spectrum of troilite which has a chemical composition close to FeS and was present in the Forest City Chondrite.

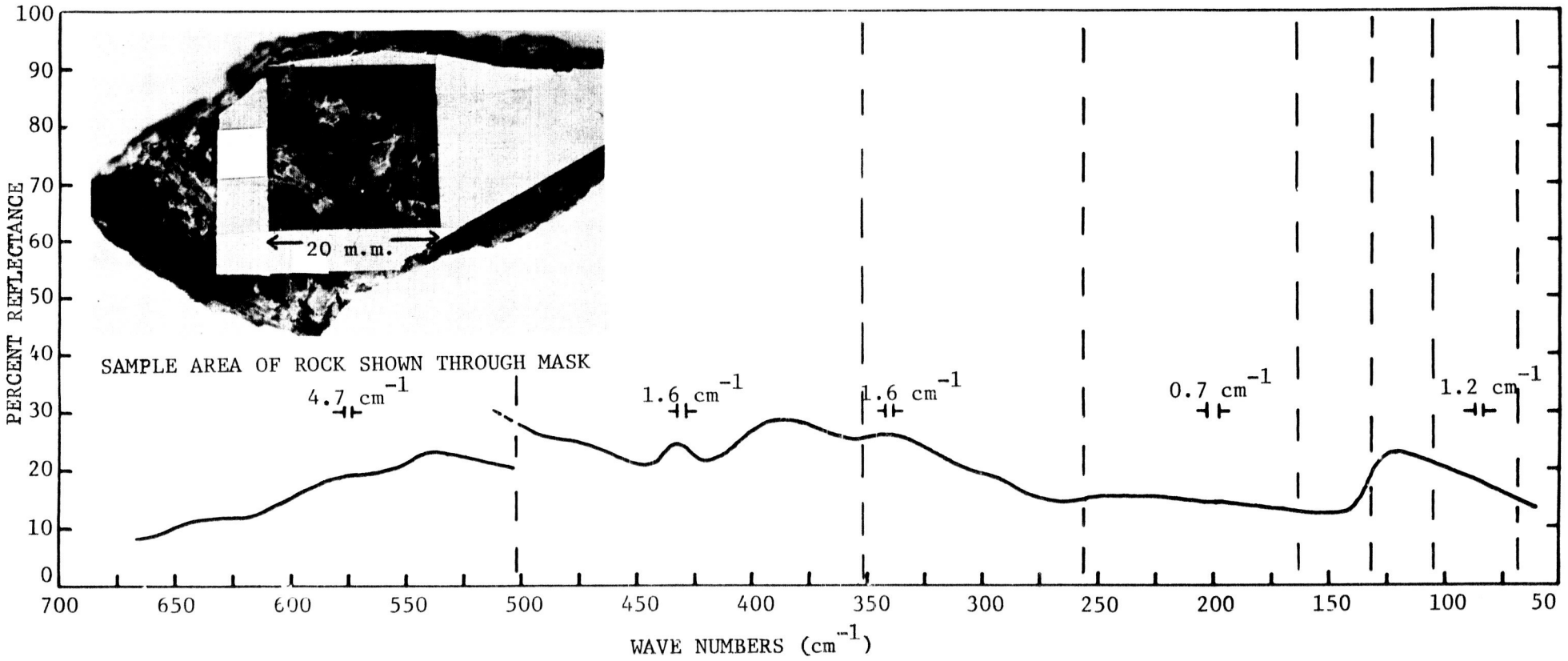

FIGURE 6. FAR INFRARED REFLECTANCE OF PIGEONITE-ANDESINE

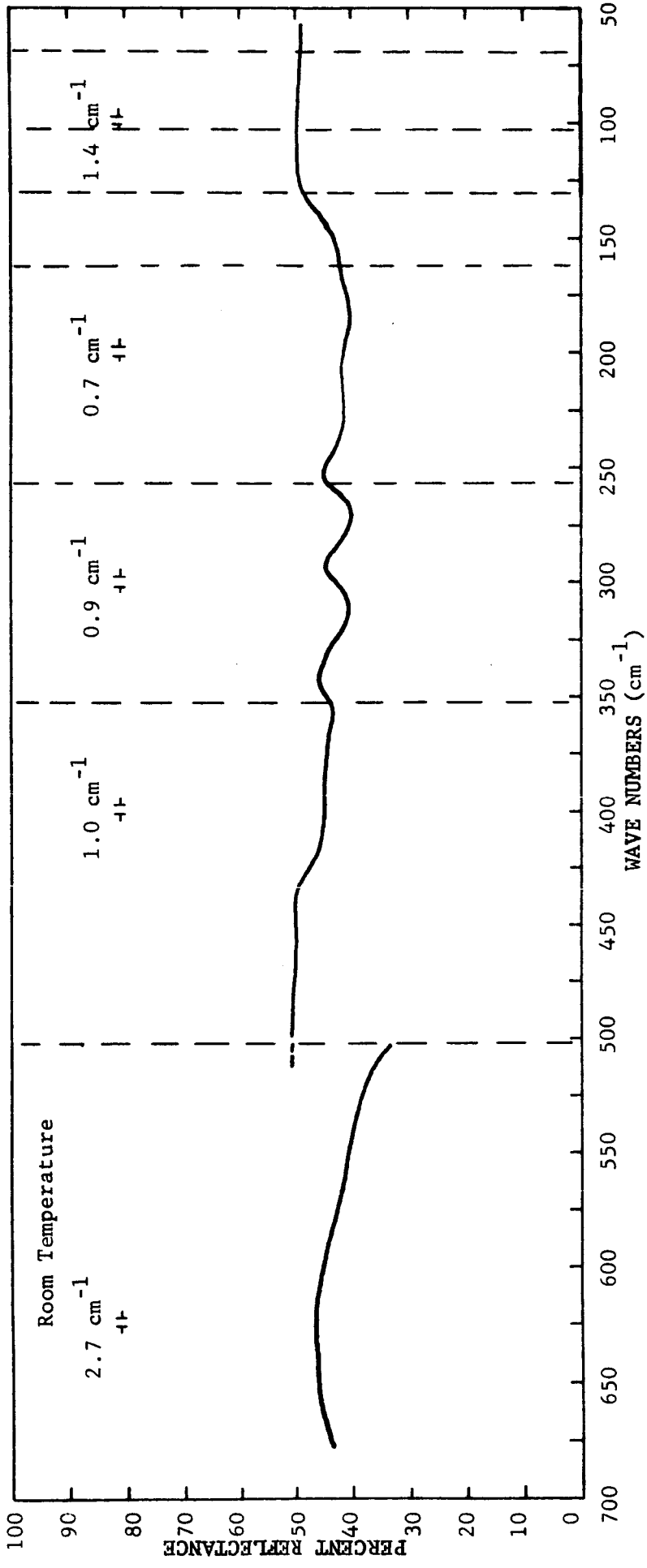

FIGURE 7. FAR INFRARED REFLECTANCE OF TROILITE

A summary of the pertinent information such as chemical composition, crystal orientation, and source for all the minerals studied is given in Table I.

G. POLARIZATION EFFECTS

It is very important to note the effects of instrumental polarization (Figure 8) on the measured spectra. As shown in the figure changes in instrumental polarization which result from the changes in optical components (shown by the dashed vertical lines) may be quite large. Our measured reflectances are given by the formula

$$R_m = 1/2\ (1 + V)\ R_\pi + 1/2\ (1 - V)\ R_\sigma \qquad (1)$$

where R_m is the measured reflectance, R_σ is the reflectance of radiation with a perpendicular orientation between the electric vector and the plane of incidence, R_π is the reflectance for the parallel component and V is the polarization of the spectrometer.

$$V = \frac{I_\pi - I_\sigma}{I_\pi + I_\sigma} \qquad (2)$$

where the I's are the intensities of radiation with a polarizer set to pass the appropriate polarized radiation. In the figure we have plotted $|V|$.

R_π and R_σ are, of course, smooth functions of frequency or wavelength but the drastic changes in instrumental polarization at, for instance, 500 cm^{-1} is a contributing factor to the spectral discontinuities often observed at this point.

By and large the other polarization discontinuities are too small to show in the measured spectra.

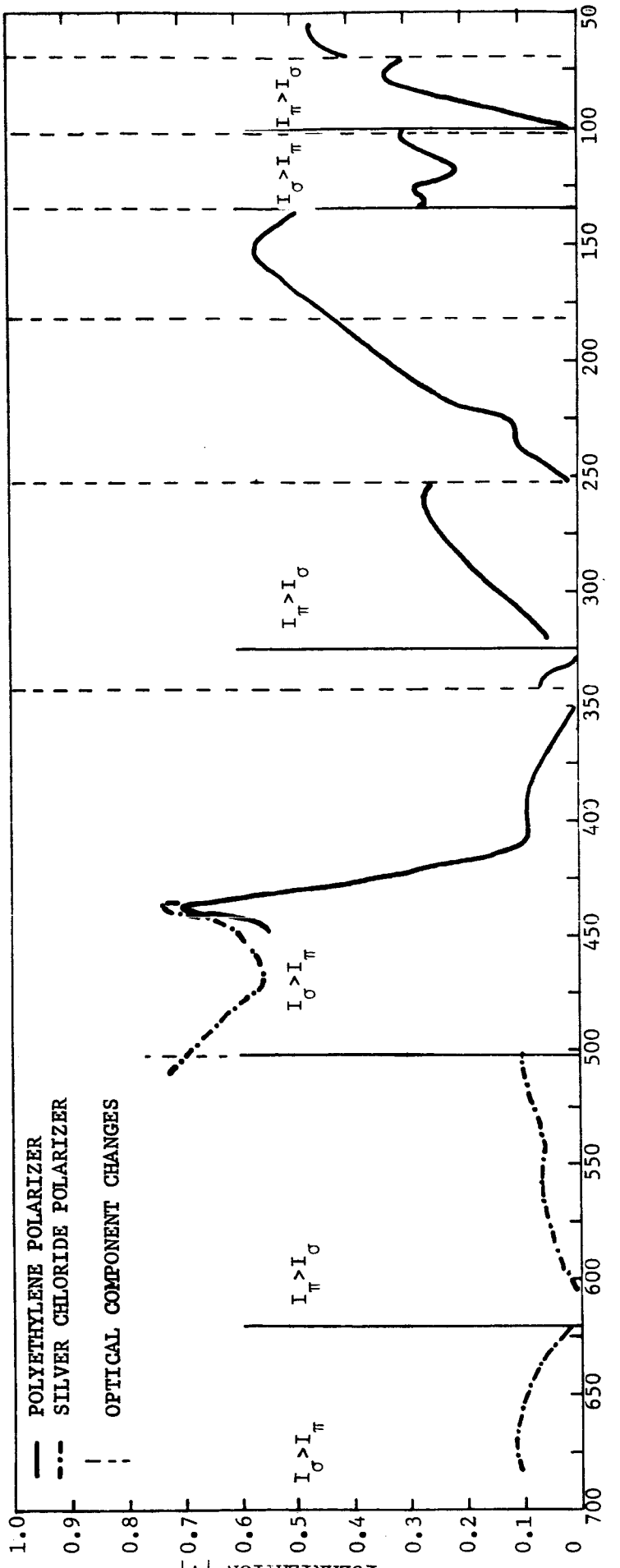

FIGURE 8. SPECTROMETER POLARIZATION

III. STATE OF SURFACE AGGREGATION

Previous studies[5] show that good spectra of high information content can be obtained by reflection or emission from bulk minerals, whether polished or rough. Coarse particulate material will give reflection spectra of increased intensity, owing to the contribution of volume reflection (See Section III,B). The reflectance is further enhanced as the particle size is reduced[13] which we believe to be the result of increased backscattering due to multiple internal reflections within the grains when the particles are larger than the wavelength. However, when the particles are made smaller than the wavelength, the reflectance falls off drastically and, therefore, the material almost appears to be a blackbody.

At the conclusion of our previous work, we were very concerned about this apparent loss of spectral details in spectra resulting from fine particulate surfaces. We proposed a theoretical investigation of this problem along with several laboratory experiments in order to try to resolve some apparent contradictions between various experimental results[1,4,14] and existing theory.

A. EXPERIMENTAL RESULTS

We began the study of the problem of spectral contrast on reflection from particulate surfaces by preparing a new sample (the original had been damaged) from our 1-micron fayalite powder as detailed in our previous work. This surface, prepared exactly as before,[1] appeared somewhat darker on visual inspection but, as samples have had this type of variability before, we proceeded with our measurements. A photograph of this sample is shown in Figure 9. A reflection spectrum of the powder surface was run on our Perkin-Elmer 521 double beam analytical spectrometer. This instrument is capable of measurements to 250 cm^{-1} although it loses sensitivity toward the end of the region. The object was to scan

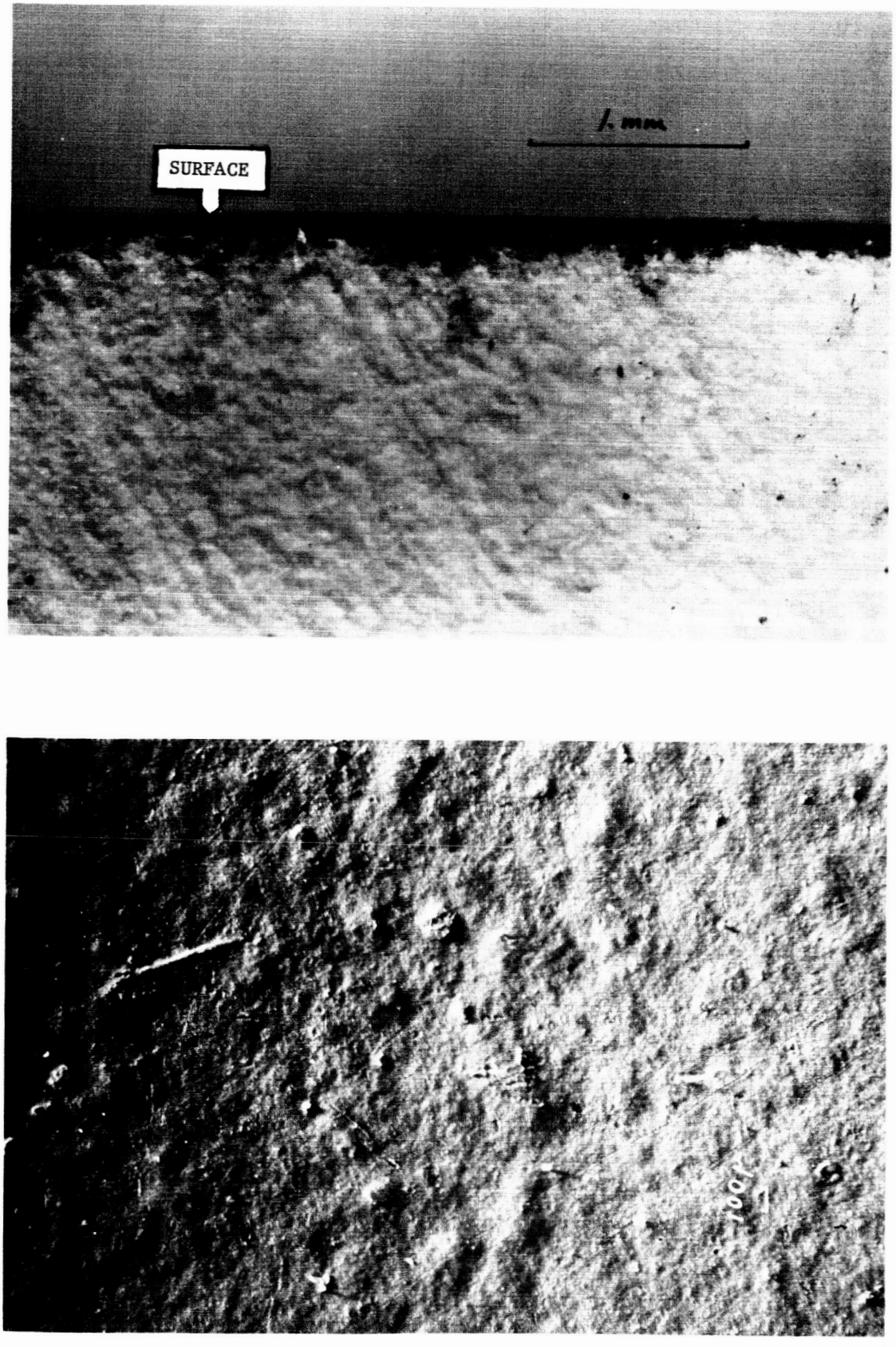

FIGURE 9. FAYALITE POWDER REFLECTING SURFACE

the spectral region in question many times in an attempt to average out the noise and so determine whether the signal actually contained the spectral contrast information present in bulk samples. It proved unnecessary to do this as, in the course of an initial run, an attenuator was placed in the reference beam, and with suitable differences in slit, gain, etc., we were able to obtain sufficient spectral contrast to recognize a somewhat displaced fayalite spectrum. This is shown in Figure 10. We proceeded to obtain a similar spectrum using our 201-C Far Infrared Spectrophotometer by making necessary adjustments in slit and gain settings. This is shown in Figure 11, along with the spectrum of bulk fayalite. It should be noted that the angle of incidence used with the 521 is 30° and with the 201-C it is 45°. Further, the polarization characteristics of the 521 are unknown and the calibration is less well known that with the 201-C. There appears to be a long wavelength shift of the spectrum using the 521 Spectrophotometer for the powder surface as compared to the bulk fayalite spectrum. The wavelength shift is difficult to explain and cannot be entirely attributed to instrumental difficulties since it does not vanish although it is perhaps somewhat reduced in the powder spectrum run on the 201-C. Nevertheless, the similarity of the spectra obtained from the two instruments is obvious. A run on the new sample under conditions similar to those used in our previous work shows that somewhat higher reflectance and enhanced spectral details are obtainable with this sample than with the original (See Figure 12). Runs made with the 521 Spectrophotometer under "more normal" conditions (without reference beam attenuation) show a comparable reflectance level of approximately 5 to 10% with some small features visible. We feel the point is amply demonstrated that spectral contrast is obtainable in reflection experiments from fine powder surfaces. The importance of these experiments is that while reflectance is reduced on going from bulk to particulate surfaces, the conclusion reached by Corliss[15], that "spectral structure is wiped out" by finely powdered substances in emission, is incorrect.

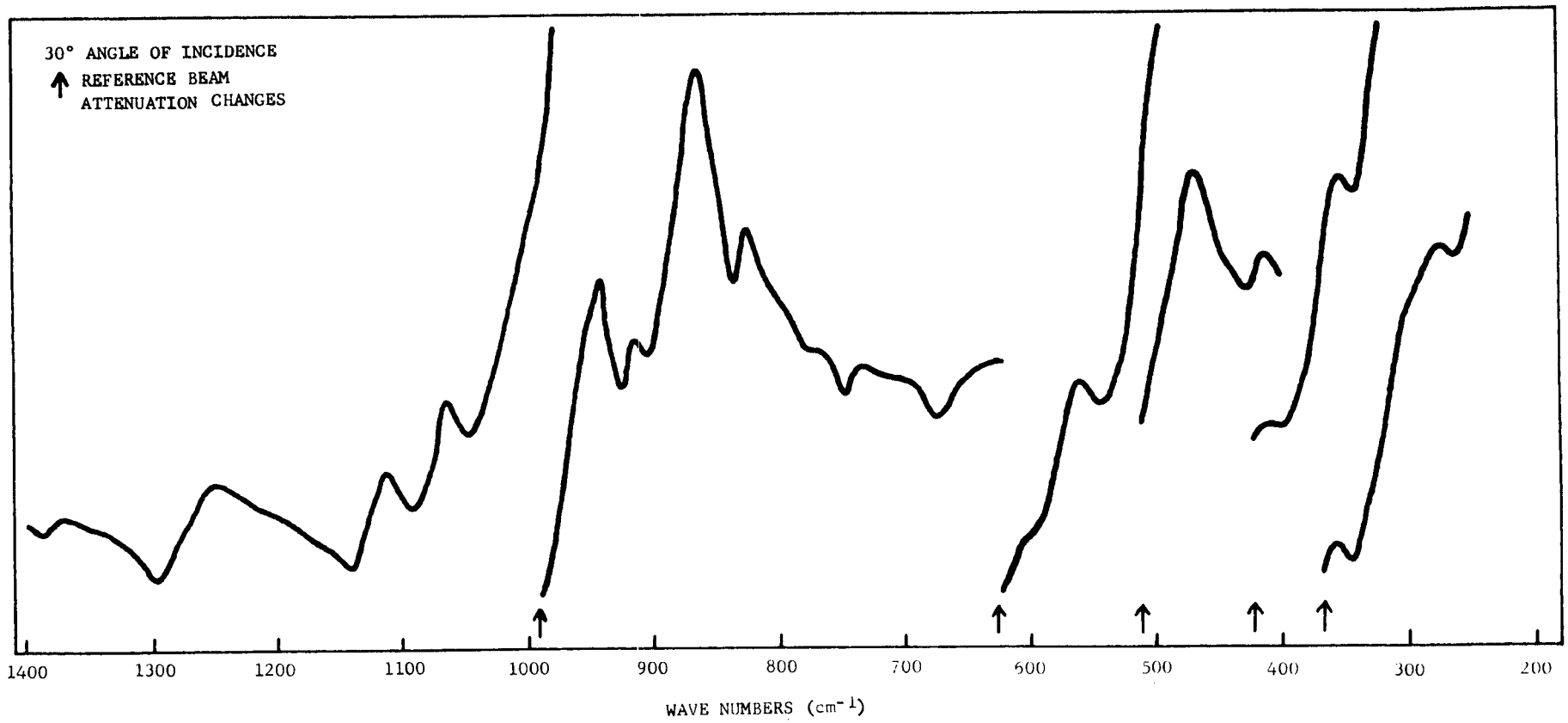

FIGURE 10. SPECTRAL DETAILS OF FAYALITE POWDER (521 SPECTROPHOTOMETER)

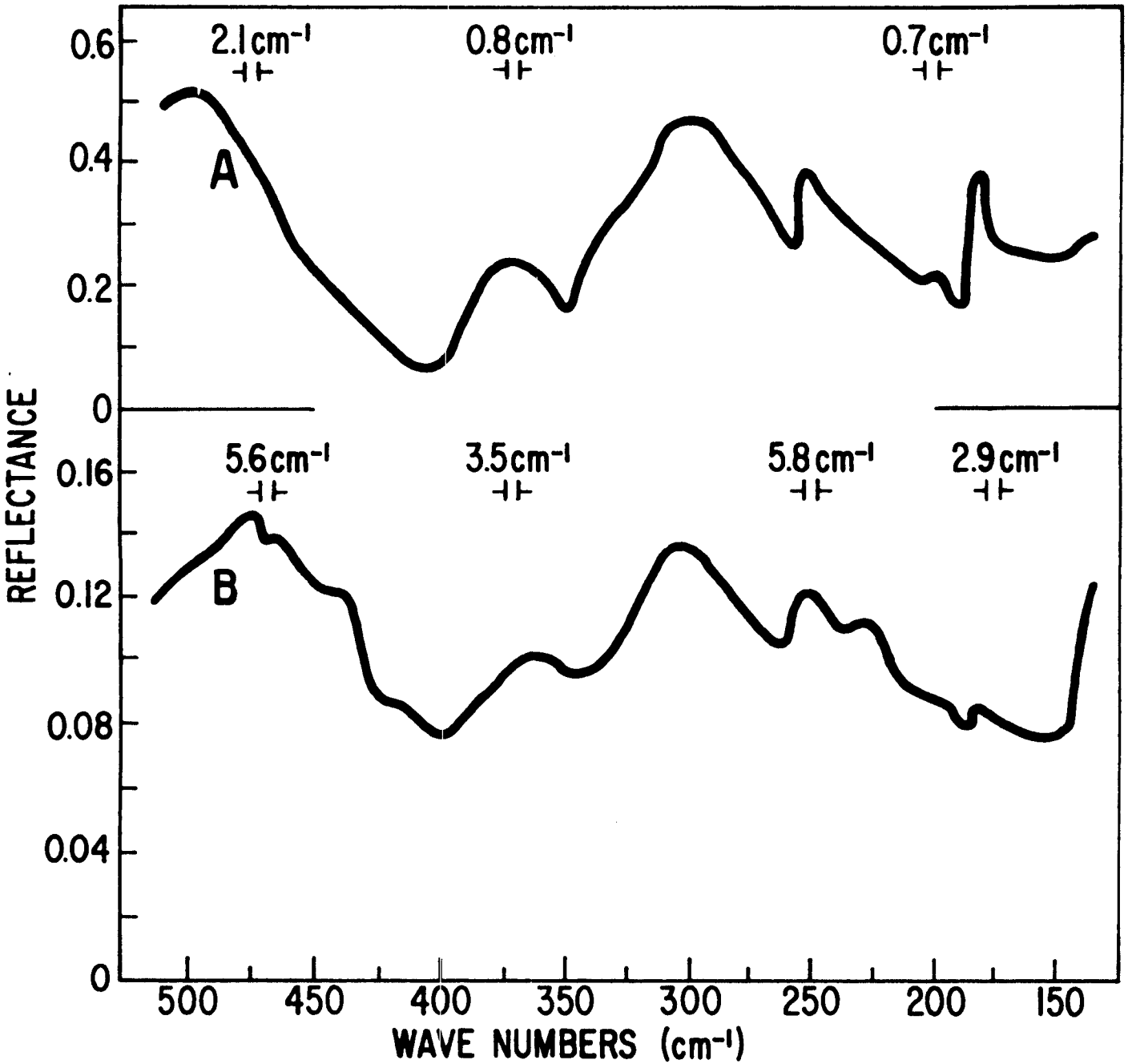

FIGURE 11. FAR INFRARED REFLECTANCE OF FAYALITE: A, BULK MINERAL; B, POWERED MINERAL
The difference in the vertical scales of the two spectra accentuates minor features, possibly spurious, in the lower spectrum.

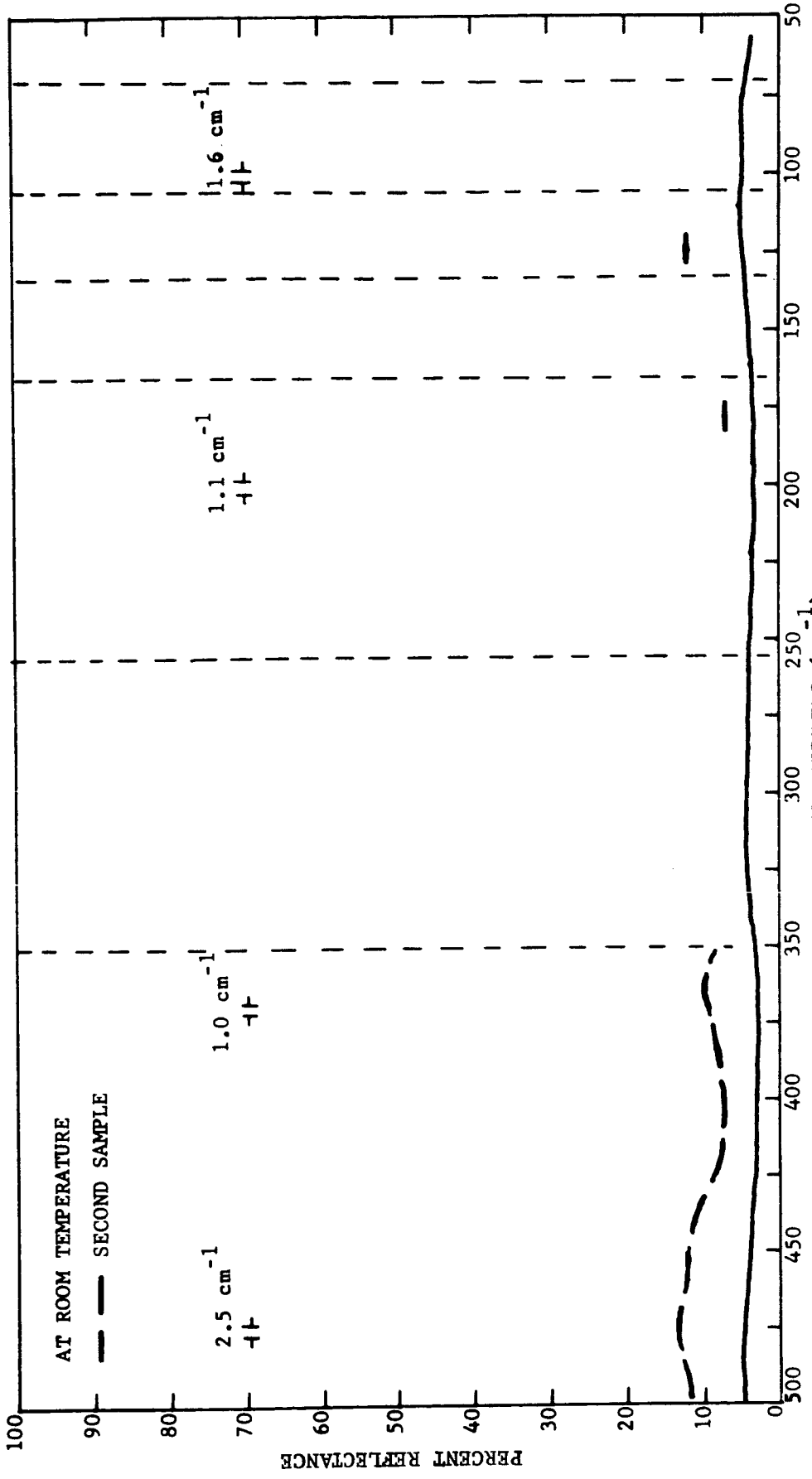

FIGURE 12. FAR INFRARED REFLECTANCE OF FAYALITE POWDER

Further powder spectra were obtained from fine particulate samples of quartz which are shown in Figure 13. These spectra were obtained with two different packing fractions (volumes) to illustrate the effect of void spaces on the spectra. The quartz powder has a particle size range from 1.6 to 5 microns and is shown in Figure 14.* The less dense sample was placed in an aluminum cup and the sample face smoothed with a spatula. This was necessary as our instrumentation is designed for making specular measurements. The denser sample was compressed somewhat by slight pressure in order to obtain a different packing volume. We feel that there is no longer any possibility of doubt that spectral details are present in fine powder samples.

We originally thought that our previous experimental results[1], as well as those of Van Tassel and Simon[14] who made emission measurements, could be explained simply on the basis of a large diffuse component to the radiation. This component might result from the gross roughness of the sample (See Figure 9) rather than the individual particle size and would have the effect of cutting down the measured signal until signal-to-noise problems made good spectral contrast measurements difficult. This assumption was tested for our experimental arrangement by comparing the reflectance level in the "specular" position with that in several "diffuse" positions of the sample. As the incident and detected beams are fixed 90° apart in our spectrometer, we rotated the sample into the incident beam for our measurements. This had the effect of giving an angle of detection equal to 90°-i where i is the angle of incidence. By turning the sample into the incident beam, we avoided any energy bypassing the sample altogether. The results are shown in Figure 15, where it can be seen that the reflected radiation falls off very rapidly as the "specular" beam is lost to the view of the detector. This experiment renders our tentative explanation of the signal loss invalid. We note

---

* Some larger particles are visible in the photograph, but numerous microscopic examinations show the bulk of the material to be in the 1.6 to 5 microns range.

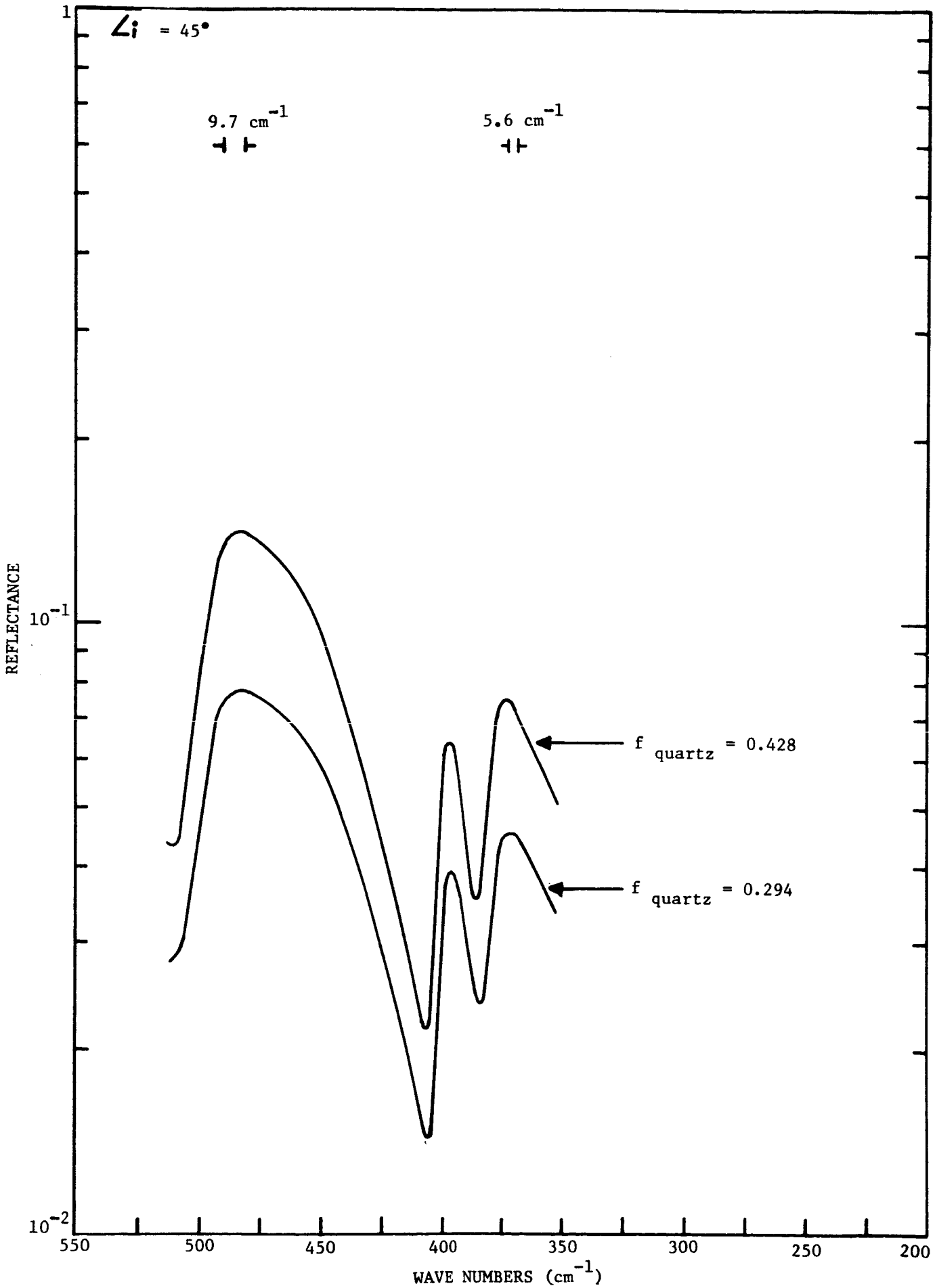

FIGURE 13. FAR INFRARED REFLECTANCE OF QUARTZ POWDER

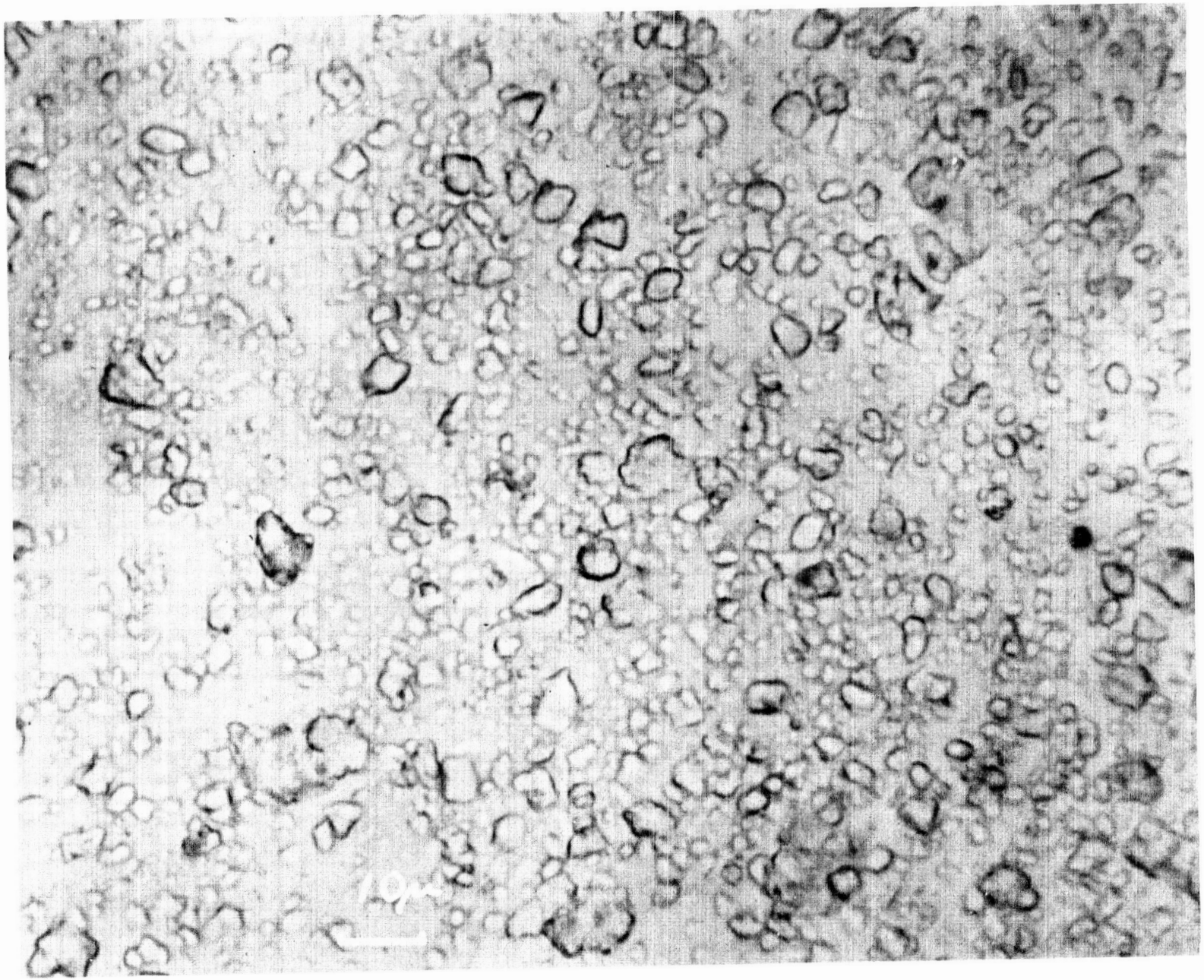

FIGURE 14. QUARTZ POWDER

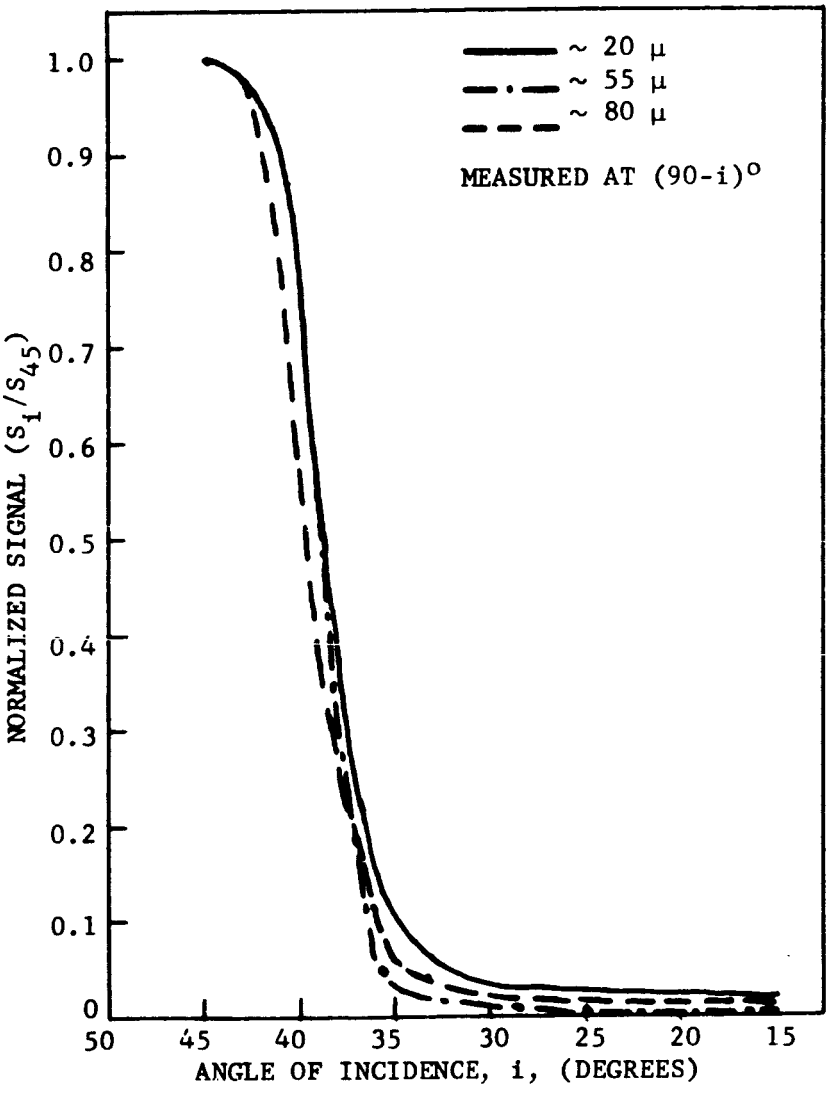

FIGURE 15. ANGULAR DEPENDENCE OF SIGNAL.

that the angular spread of the "specular" beam is similar to what we expected, judging by the optical diagram of our instrument. Therefore our sample is essentially a specular reflector.

We were left with the conclusion that spectral details can be discerned in reflection from particulate media and, by implication, by proper use of Kirchhoff's Law, in emission. However, the experimental observations of lessened reflection and less easily observed spectral details remain.

Our explanation of these phenomena is based upon packing density rather than particle size. It is true, however, that fine particles generally pack rather loosely. As is well known, reflectivity is given in terms of the optical constants of the medium, n and k, by the Fresnel equations of which the simplest is, at normal incidence

$$R = \frac{(n - 1)^2 + k^2}{(n + 1)^2 + k^2} \tag{3}$$

If the material in question is in large measure made up of voids, then n and k should be replaced by effective optical constants where these quantities are averaged over the material and the vacuum. As a first approximation when the complex refractive index, n - ik, is close to 1, the average index is given by[16]

$$\bar{n} - i\bar{k} = f(n - ik - 1) \tag{4}$$

where f is the packing density, or the fraction of the volume occupied by the particles. This leads to the equation*[17]

$$R = \frac{(n - 1)^2 + k^2}{(n + \frac{2}{f} - 1)^2 + k^2} \tag{5}$$

* The theoretical derivation of this expression is given in the following section.

An example shows the type of effect to be expected. For n = 1.5 and k = 1, R for the bulk material would be 0.172 or 17.2%. For the same material with 50% of the bulk density, R would be 0.059 or 5.9% (see next section). A rough check on the density of our material gave d ~ 2.5 as opposed to d = 4.14 for bulk fayalite. It is possible that such a phenomenon could explain Lyon's[5] data for 200Å Al_2O_3. He described his technique as compacting the material so that it would stay in his vertical sample holder. We attempted to simulate this with 500Å Al_2O_3 powder in a similar holder and found that the powder will stay in a vertical position under a large range of densities, including 0.1 of that of the bulk material. This would give an even greater reduction in reflectance or increase in emittance. We observe that the actual emittance value given by Lyon for his 200Å powder is very close to blackbody, being derived from a very low reflectance value by means of Kirchhoff's Law. In principle this type of dilution effect does permit the retention of some spectral contrast as we discuss in the next section.

When n - ik is not close to 1, no simple equation for reflectance is obtained. In its place we have derived the following mixing rule based on the Lorentz-Lorenz theory of dielectrics.

$$\frac{(\bar{n} - i\bar{k})^2 - 1}{(\bar{n} - i\bar{k})^2 + 2} = f \frac{(n - ik)^2 - 1}{(n - ik)^2 + 2} \qquad (6)$$

We will discuss a generalized form of this equation and show its derivation in a later section of this report. The "averaged" optical constants may then be used with the Fresnel equations to compute reflectance for a fine particulate surface.

B. THEORY OF THE SPECTRAL REFLECTANCE OF A SEMI-INFINITE PARTICULATE MEDIUM[18]

Considerable insight into the spectral reflectance characteristics of a particulate medium can be obtained by means of a simple model

in which diffuse radiation is reflected from a semi-infinite medium composed of randomly distributed spherical particles of uniform diameter. For such a model the reflectance, in general, depends on the wavelength λ of the radiation, the optical constants $n(\lambda)$ and $k(\lambda)$ of the material of which the particles are composed, the diameter d of the particles, the average center-to-center spacing D of the particles, and the condition of the surface of the medium. The reflectance, in general, consists of both a volume and a surface contribution.

The volume contribution arises from incoherent scattering by the particles and predominates when the medium consists of widely-spaced particles of any size, as in a cloud or gas, or of closely-spaced particles of size larger than a wavelength.

The surface contribution has both a coherent component--the specular reflection, and an incoherent component--the diffuse reflection. The relative magnitudes of the two surface components depend on the roughness of the surface. Surface reflection predominates over volume reflection when the medium consists of closely-spaced particles of size much less than a wavelength.

1. Volume Reflection

The conditions for predominantly volume reflection are represented schematically in Figure 16 where diffuse incident radiation is represented by the symbol 1 and diffuse reflected radiation by the symbol R_v. The sinusoidal wave on the right indicates that the wavelength of the radiation is small compared with the particle diameter. The packing density of the particles is so low that the surface reflection effect to be discussed later is negligible compared with the volume effect.

The distribution of the spherical particles shown in the diagram is meant only to indicate the average spacing and would therefore,

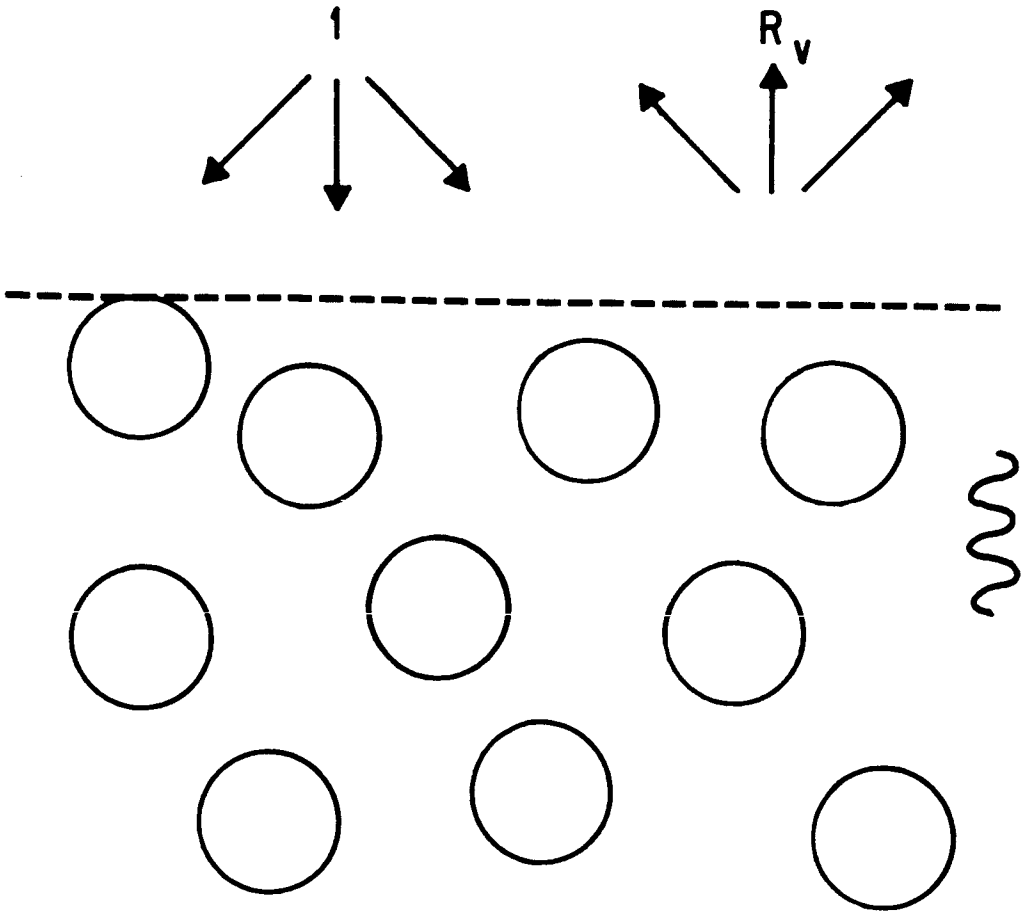

VOLUME REFLECTION

FIGURE 16.

for example, represent approximately the case of a "fairy castle" structure composed of a very porous network of particles of size considerably larger than the wavelength of the radiation. An experimental justification for this model of the fairy-castle structure is to be found in the work of Blevin and Brown[19] who found that the reflectance of a powder composed of particles larger than the wavelength was almost independent of the particle spacing over a range from very wide spacing down to spacings where the particles were almost in contact.

Volume reflection can be evaluated most simply by the two-beam theory of Schuster[20] in which forward and backward radiation fluxes I_+ and I_- represent the state of the radiation at any point in the medium, a distance x from the surface. The differential equations for I_+ and I_- are:

$$\frac{dI_+}{dx} = -(K + S)I_+ + SI_- \tag{7}$$

$$-\frac{dI_-}{dx} = -(K + S)I_- + SI_+ \tag{8}$$

where K and S are the macroscopic absorption and backscattering coefficients of the medium.

The general solution of the simultaneous first-order differential equations 7 and 8 can easily be shown to be:

$$I_+ = Ae^{x\sqrt{K^2 + 2KS}} + Be^{-x\sqrt{K^2 + 2KS}} \tag{9}$$

$$I_- = A\left(1 + \frac{K}{S} + \sqrt{\frac{K^2}{S^2} + 2\frac{K}{S}}\right)e^{x\sqrt{K^2 + 2KS}}$$

$$+ B\left(1 + \frac{K}{S} - \sqrt{\frac{K^2}{S^2} + 2\frac{K}{S}}\right)e^{-x\sqrt{K^2 + 2KS}} \tag{10}$$

In the case of a semi-infinite medium, I_+ and I_- must approach zero for large x. Thus A = 0. The reflectance R_v can then be evaluated as the ratio of I_- to I_+ at x = 0:

$$R_v = 1 + \frac{K}{S} - \sqrt{\frac{K^2}{S^2} + 2\frac{K}{S}} \tag{11}$$

It is noteworthy that the reflectance depends only on the ratio K/S of the absorption and back-scattering coefficients. Now, when the particles are, on the average, far enough apart that they act essentially independently, one can write

$$K = N \sigma_a \tag{12}$$

$$S = N \sigma_s$$

where N is the number of particles per unit volume, σ_a is the absorption cross-section, and σ_s is the back-scattering cross-section of a single particle. Thus

$$\frac{K}{S} = \frac{\sigma_a}{\sigma_s} \tag{14}$$

and from equation 11

$$R_v = 1 + \frac{\sigma_a}{\sigma_s} - \sqrt{\left(\frac{\sigma_a}{\sigma_s}\right)^2 + 2\frac{\sigma_a}{\sigma_s}} \tag{15}$$

This expression shows that the reflectance is independent of the number of particles per unit volume, in accord with the experimental results of Blevin and Brown[19], and is a function only of the ratio of the two cross-sections of a single particle. Figure 17, which is a plot of equation 15, shows that R_v decreases quite rapidly at first as the ratio of absorption to scattering cross-section increases, but then falls off more slowly when σ_a/σ_s exceeds 1.

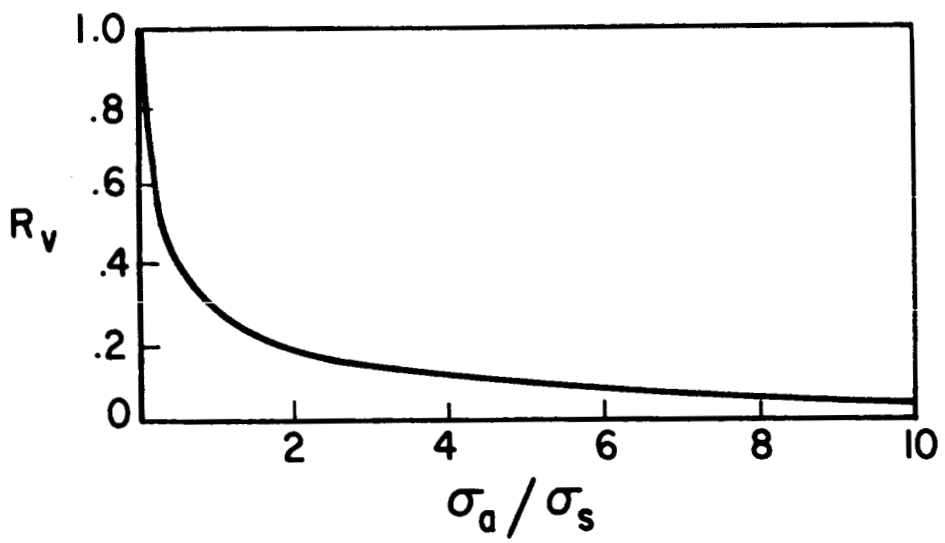

FIGURE 17. VOLUME REFLECTION vs RATIO OF ABSORPTION AND SCATTERING CROSS SECTIONS

In principle, the ratio σ_a/σ_s could be calculated as a function of wavelength by means of the scattering theory of Mie for any given dependence of the complex index of refraction n - ik on wavelength. In practice, however, the computation would be very difficult because σ_s is the cross section for scattering into the backwards hemisphere and not the total scattering cross-section that is relatively easy to derive from the Mie theory.[16] Therefore only a qualitative discussion will be given about the dependence of σ_a/σ_s on $n(\lambda)$, $k(\lambda)$, and d/λ.

Of great interest is the way in which σ_a/σ_s (and therefore R_v) depends on the absorption index $k(\lambda)$. In the limiting case of perfectly transparent particles for which $k = 0$, the ratio σ_a/σ_s is zero since no absorption occurs within the particles. Thus, from Figure 17, $R_v = 1$. In the other limiting case of perfectly reflecting particles for which $k = \infty$, σ_a/σ_s is again zero since no energy can enter the particles and be absorbed. Therefore, $R_v = 1$ in this case, also. The dependence of R_v on k must therefore, in general, resemble the curve in Figure 18a in which R_v approaches 1 for some intermediate value k_1 for which σ_a/σ_s is a maximum. The minimum of the R_v curve in Figure 18a means that two types of absorption bands should be distinguishable in the volume reflection spectra of particulate media. A weak band for which k is less than k_1 throughout the band will appear as a dip in the spectral reflectance curve, as shown in Figure 18b, because R_v decreases as $k(\lambda)$ increases. On the other hand, a strong reststrahlen band for which k becomes greater than k_1 over part of the band will appear with the opposite polarity as in Figure 18c, since R_v now increases with increasing k, according to Figure 18a. The two kinds of bands can be called dielectric-type bands and metallic-type bands, respectively. The experimental results of Blau and Espinola[21] on the reflection of infrared radiation by clouds of large ice particles ($d \sim$ 50-100 microns) appear to show both kinds of bands. At the centers of the relatively weak bands near 1.5 microns and 2 microns the radiation reflected from the cloud is lower than at adjacent wavelengths, while the reverse is true for the very much stronger reststrahlen band at 3.1 microns. One may expect to find similar behavior

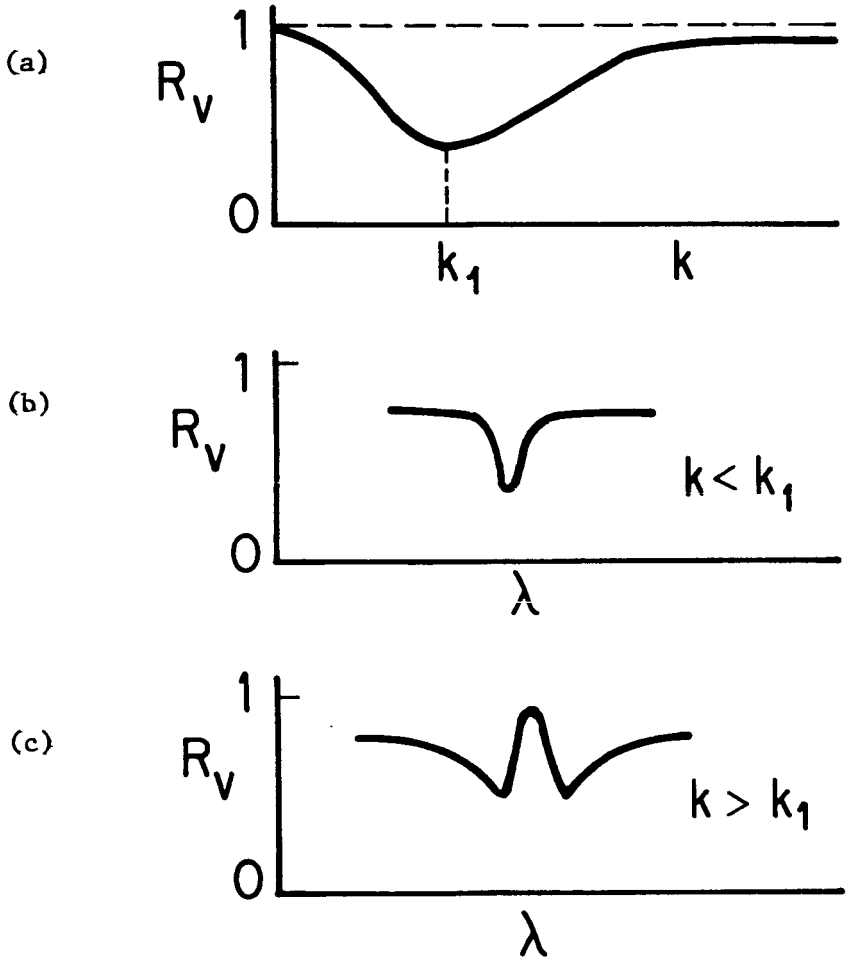

FIGURE 18. VOLUME REFLECTION FOR STRONG AND WEAK RESONANCES

in the reflection spectra of coarse powders, such as silica sand. It is to be noted that the strong reflection bands have the same polarity as the bands in the reflection spectra of homogeneous solids.

2. Surface Reflection

Surface reflection predominates over volume reflection under the two conditions illustrated in Figure 19.

In Figure 19a the particles of a coarsely divided medium have been compressed so closely that the residual voids are small in size compared both with the particles and with the wavelength of the radiation Under these circumstances the volume scattering, which now results from the small widely-spaced voids in an otherwise continuous medium, is much less than the Fresnel reflection arising from the discontinuity in the optical constants at the surface of the medium.

Figure 19b represents the case of a fine powder where the particle size and spacing are both small compared with the wavelength. Volume reflection is negligible in this case because σ_a/σ_s is generally very large in the Rayleigh scattering region for materials that have a finite absorption index. However, the surface reflection is important since large numbers of particles act cooperatively when the interparticle separation is much less than a wavelength. This coherent effect is entirely equivalent to the effect of the discontinuity in the average complex refractive index at the surface of the medium. When the index $n - ik$ of the individual particles is fairly close to 1, the space-averaged index $n - ik$ is given by[16]

$$(\bar{n} - i\bar{k} - 1 = f(n - ik - 1) \qquad (4)$$

where f is the packing density, i.e., the fraction of the volume occupied by the particles. On equating real and imaginary parts of equation 4, one obtains:

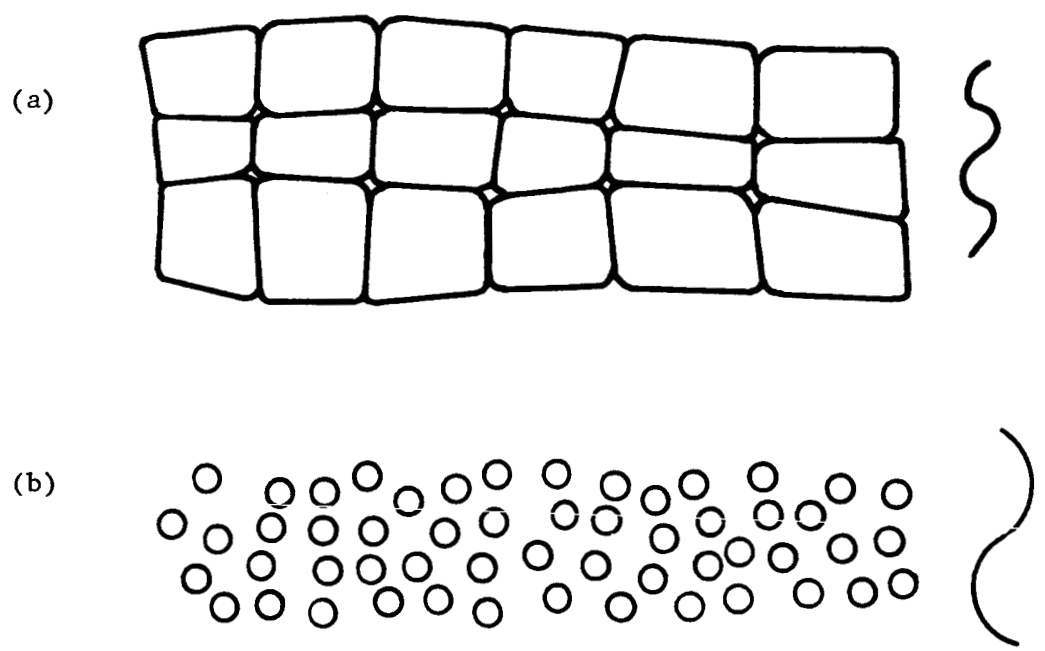

FIGURE 19

$$\bar{n} - 1 = f(n - 1) \tag{16}$$

$$\bar{k} = f\,k \tag{17}$$

An approximate estimate of the diffuse surface reflectance R_s is obtained if expressions (16) and (17) are substituted into the simple Fresnel formula for normal incidence

$$R_s = \frac{(\bar{n} - 1)^2 + \bar{k}^2}{(\bar{n} + 1)^2 + \bar{k}^2} \tag{18}$$

One then finds

$$R_s = \frac{(n - 1)^2 + k^2}{(n + \frac{2}{f} - 1)^2 + k^2} \tag{19}$$

Table II shows the effect of the packing density f on the reflectance R_s and on the spectral contrast $(R_s)_{max}/(R_s)_{min}$ for the case of a fairly strong absorption band in which we assume for simplicity that the refractive index n remains constant at 1.5* while the absorption index increases from 0 to 1 between the edge and center of the band. The table shows that the reflectance at the center of the band decreases markedly from 17% to 0.3% when the packing density decreases from 100% to 10%. But the spectral contrast, which is the ratio of the reflectance at the center of the band to the reflectance at the edge of the band, remains high and actually increases with the dilution of the powder. Thus if high signal-to-noise ratio can be obtained in the measurement of spectral reflectance, either by slow scanning with relatively wide slits in a spectrometer, or by the use of an interferometer, there appears to be no reason why excellent reflection spectra should not be obtainable from finely-divided low-density powders.

---

* As n actually undergoes anomalous dispersion in the region of an absorption band, the results of a more comprehensive calculation will be given in Section IV.

TABLE II

THE EFFECT OF PACKING DENSITY ON SURFACE REFLECTANCE AND SPECTRAL CONTRAST FOR CONSTANT REFRACTIVE INDEX

f	n	k	R_s	$(R_s)_{max}/(R_s)_{min}$
1	1.5	0	.04	4.3
1	1.5	1	.172	
0.5	1.5	0	.0123	4.8
0.5	1.5	1	.059	
0.1	1.5	0	.0006	5.0
0.1	1.5	1	.003	

It is worth noting from equation 19 that for constant n, R_s always increases with increasing k. Thus the surface reflection spectrum of a fine powder has the same polarity as the reflection spectrum of the bulk material, but it has opposite polarity to the volume reflection spectrum of weak bands from a coarse powder.

3. Effect of Surface Roughness

Surface roughness can have an important effect only on the surface contribution to the reflection by a particulate medium. Thus the diffuse reflectance of a medium composed of coarse particles, such as sand or a cloud of large ice crystals, is not affected appreciably by the state of the surface of the medium.

In the case of a medium of fine particles, where the reflection is caused almost entirely by the surface discontinuity in the optical constants, the state of the surface can be important under certain conditions. If the surface contains no steep-walled cavities of dimensions comparable with the wavelength, roughness merely causes a redistribution

in angle of the reflected radiation but does not change the total amount of energy reflected. Thus the diffuse reflectance is independent of gentle surface irregularities. Reduction in the reflectance begins to occur when the surface is so rough that an appreciable fraction of normally-incident rays suffer a double bounce. In general, if $R_0(\lambda)$ is the average reflectance for a single bounce, then the reflectance of the rough surface is approximately

$$R = F_1 R_0(\lambda) + F_2 R_0^{\,2}(\lambda) + F_3 R_0^{\,3}(\lambda) + \ldots \qquad (20)$$

where F_1, F_2, ... are the fractions of the radiation undergoing single, double, etc., bounces.

In the critical case of a fine powder of low packing density, $R_0(\lambda)$ is quite small, and all terms in equation 20 except the first can be neglected. Thus the reduction in reflectance due to roughness is simply the fraction F_1 of incident rays that make a single bounce. This fraction is moderately large except when the geometry of the roughness is exceedingly angular.

It is worth noting that when $R_0(\lambda)$ is not small, as in the case of solid material or wind-packed powder, roughness changes the shape of the spectrum since the multiple-bounce terms in equation 20 are nonlinear in $R_0(\lambda)$. The effect sharpens the spectral peaks.

4. Determination of Packing Density and Particle Size

The theory outlined above leads to the following conclusions:

a. When the wavelength is much smaller than the particle size, the reflectance depends mainly on volume scattering and is independent of packing density.

b. When the wavelength is much larger than the particle size, the reflectance is a surface effect and decreases rapidly with packing density.

These theoretical results imply that the spectral reflectance of a powder should have a relatively high average level, comparable with that of the bulk material, for wavelengths less than the particle size, and that the level should drop to a lower average value for wavelengths larger than the particle size. The wavelength at which the change in level occurs therefore determines the particle size, while the reflectance level itself at the longer wavelengths, in conjunction with known values of the optical constants, determines the packing density.

An experimental search for the change in emittance (or reflectance) level was carried out using a double beam emissometer in which the reference beam was derived from a "black" surface emitter radiating at approximately the same temperature as the sample. The radiation from both the sample and the reference is integrated over a solid angle of approximately 1.5π by means of a gold-plated hollow collector and conducted by a light pipe to the slits of the double-beam monochromator of our Perkin-Elmer 521 spectrophotometer. The sample was the quartz powder previously mentioned having a particle size range from 1.6 to 5 microns. The results of a qualitative experiment are shown in Figure 20. The expected emittance rise appears between 3.5 and 6 microns. The sample temperature was nominally 220°C. A broad emittance minimum is visible in the region between 7 and 10 microns, corresponding to a reststrahlen feature for this material shown in the insert.

The relatively small emittance minimum can probably be understood in terms of the foregoing discussion of the effect of low packing density on the spectra of sub-wavelength size particles. Although the packing density was not measured in the emission experiment, we infer a similar magnitude to that given in Figure 13. Therefore an emittance of approximately 0.95 ± 0.03 is expected in the region of this reststrahlen.

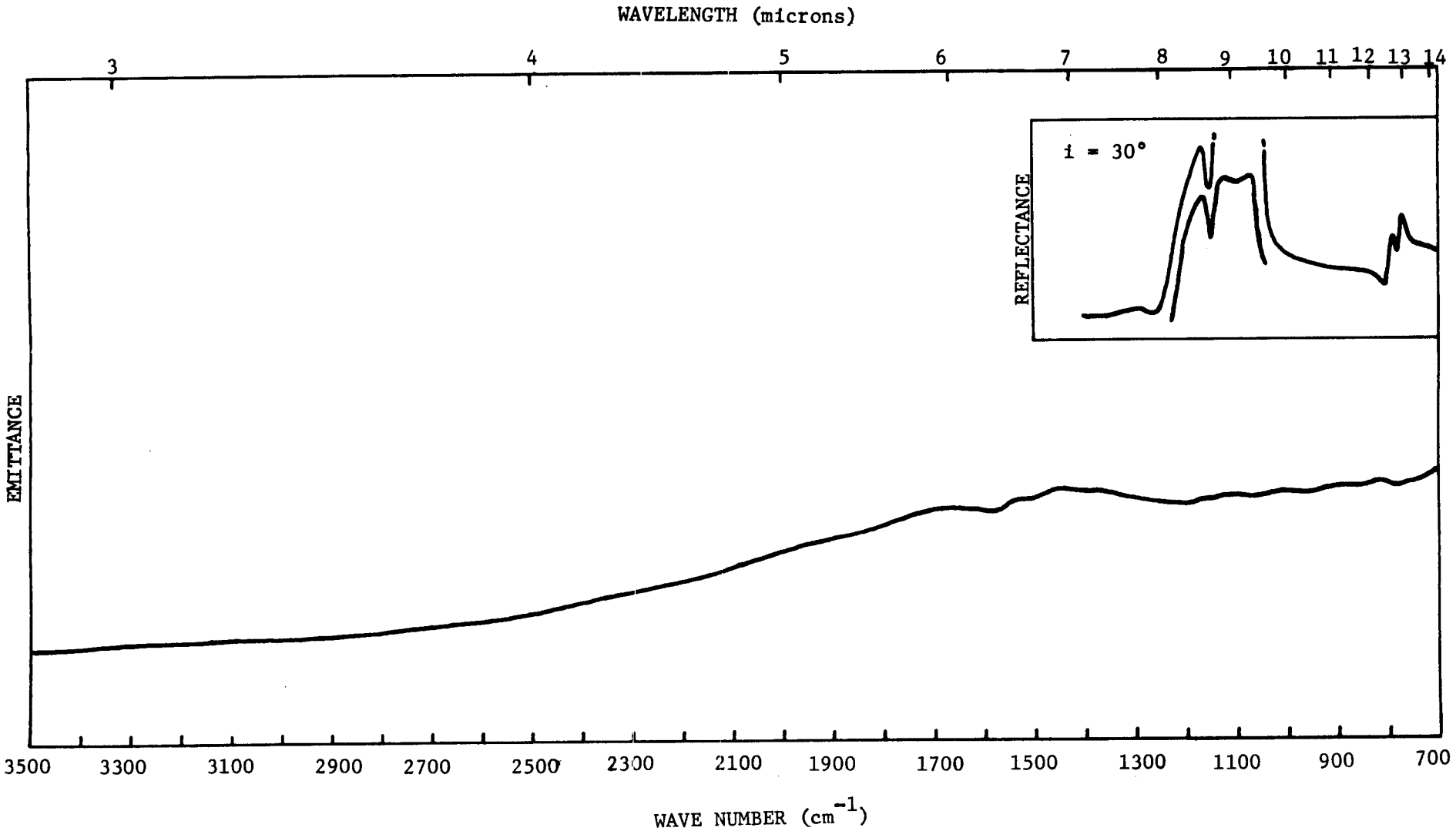

FIGURE 20. QUALITATIVE INFRARED SPECTRA OF QUARTZ POWDER (521 SPECTROPHOTOMETER)

On this basis a blackbody curve at the sample temperature would be expected to lie only slightly above the longer wavelength part of the emittance curve shown in Figure 20. Under these conditions a signal-to-noise ratio higher than that employed would be necessary to show the details of the spectrum which can be seen in the insert reflection spectrum of the same powder. This point will be further discussed in Section V. Further work needs to be done here, but we are gratified by the appearance of the predicted emittance change at a wavelength near the particle size.

IV. MIXTURES OF MINERALS

In general, one may expect the spectrum from the surface of a planet to be that of a composite owing to the size of the areal resolution element that follows from system design considerations. For example, in our recent proposal[2] of a broadband infrared interferometer for the 1971 Voyager Mission to Mars the resolution element had a diameter of about 100 km. An area of this size could contain a number of different mineral species, some in the form of spatially separated bare rocks, others mixed together in patches of fine dust. The spectral mixing rules are quite different in the two cases.

If the minerals are spatially separated either in distinct rocks or in large grains in a single rock, the individual reflectances add linearly with weighting factors proportional to the respective areas. We have tested this simple rule using a chondrite composed of seven minerals (including four silicate minerals).

A. RESULTS

We had previously run the spectrum of the Forest City Chondrite. It was our intention to measure the spectra of its component minerals and compare them, using some sort of simple mixing rule with the spectrum of the composite chondrite. Unfortunately, it proved very difficult to obtain precisely the same minerals as those reported for the chondrite.[1,22,23] In addition it was very difficult to get a good polish on the chondrite which is composed of materials of varying hardness. During the current contract, however, we succeeded in obtaining a better polish on the chondrite. This resulted in an approximately constant increase in the reflectance level of the chondrite spectrum by about 6%.

Figure 21 shows the comparison of the repolished chondrite spectrum with two calculated composite spectra on a volume per cent basis.

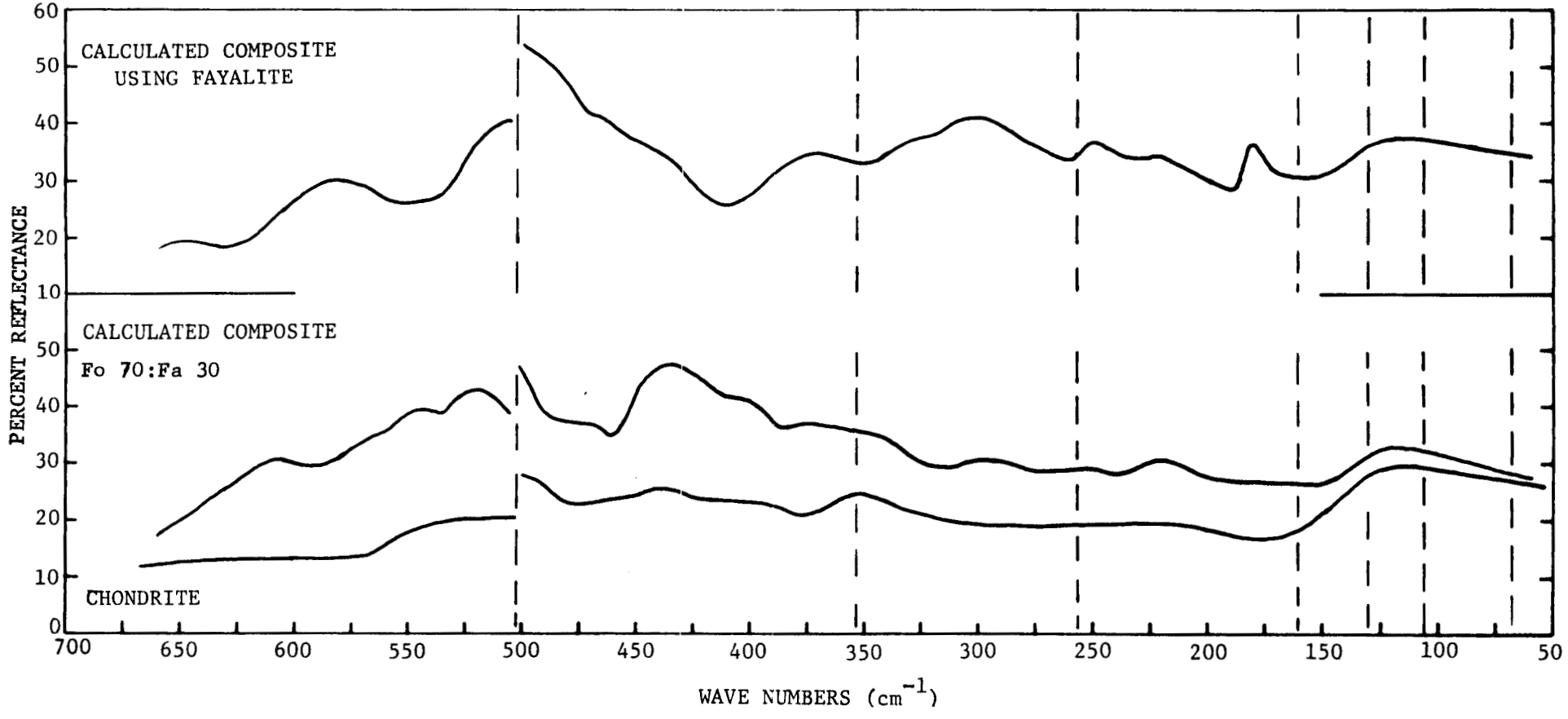

FIGURE 21. COMPARISON OF CHONDRITE SPECTRUM AND CALCULATED COMPOSITE SPECTRA

The mixing rule used assumed that the reflectances of the components could be simply added and normalized by the volume percentages of the minerals present. We believe this rule adequate if the facets of individual components are large compared with the wavelength of the radiation (which is true for much of the chondrite).

This figure demonstrates how good a match may be obtained when the proper minerals are used with a linear mixing rule. The top two spectra were obtained in precisely the same way, involving the same assumptions except for the member of the olivine series used. The top spectrum includes fayalite and the middle spectrum includes $Fo_{70}Fa_{30}$. The match obtained for the latter spectrum with the chondrite ($Fo_{81.7}Fa_{18.3}$) is, in our opinion, a demonstration of the general validity of the method used, especially when contrasted with the very poor match obtained when fayalite is used for the olivine component of the chondrite. We feel that the minor differences observed between the spectrum of the chondrite and the calculated spectrum based on $Fo_{70}Fa_{30}$ can be easily accounted for by the approximations we made in the computations. By using a flat value of 100% reflectance for the kamacite and taenite we undoubtedly calculated too high a reflectance level for our composite spectrum. The general problems of scattering by interfaces in the chondrite, orientation uncertainties for the minerals in the chondrite, and uncertain uniformity of composition throughout the chondrite can further contribute disparities between the spectra. The enstatite used was a single crystal, and the face studied is unlikely to be the orientation of that mineral in the chondrite. With natural materials, it is quite difficult to obtain specimens of exactly the same mineral composition as are present in the chondrite. As we were never able to obtain a sufficiently large sample of pigeonite, we had to substitute a feldspar (andesine)--pigeonite composite. Unfortunately, andesine has a slightly different composition than the feldspar (oligoclase) in the chondrite. Finally, the simple mixing rule used is valid only for large grains and there is some fine grained material in the chondrite. By microscopic examination, we have concluded that the bulk of the material

is large compared with the wavelength. Despite these qualifications, the good agreement in the shape of the curve for the chondrite and for the calculated composite leads us to believe that a linear mixing rule is appropriate for composite spectra if the grain size is large compared with the wavelength.

On the other hand, if the grains of different components are small, we have derived the following mixing rule (see next section).

$$\frac{(n - ik)^2 - 1}{(n - ik)^2 + 2} = \sum_p f_p \frac{(n_p - ik_p)^2 - 1}{(n_p - ik_p)^2 + 2} \qquad (21)$$

where n_p and k_p are the optical constants of the mineral of type p (including vacuum) and f_p is the volume fraction associated with each one. This rule is a generalization of equation (6) for composite samples.

A computer program was written to calculate reflectance at normal incidence using the above mixing rule to derive the average optical constants of a mixture of minerals. As a test case, we used data for X and Z-cut quartz taken from a dispersion analysis carried out by Spitzer and Kleinman.[24] Using the dispersion parameters that they obtained, the computer program recomputed the optical constants of quartz in order to avoid errors in reading data points from their graphs. The optical constants were used with equation 21 with varying f_p's to show the effect produced by changing packing fractions. However, the f for Z-cut quartz was always taken as one half of the f for X-cut quartz as the latter orientation is doubly degenerate, and a random mixture should have twice as many crystallites X-oriented as Z-oriented. Quartz is a particularly good substance to test this relationship for it fractures conchoidally. A powdered sample therefore should have no preferred orientation. In Figure 22, we show the reflectance of Z-cut and X-cut quartz and that computed for the random mix. It should be noted that the mixing rule always predicts the proper number of spectral features if one judges by the features in the component minerals, although some

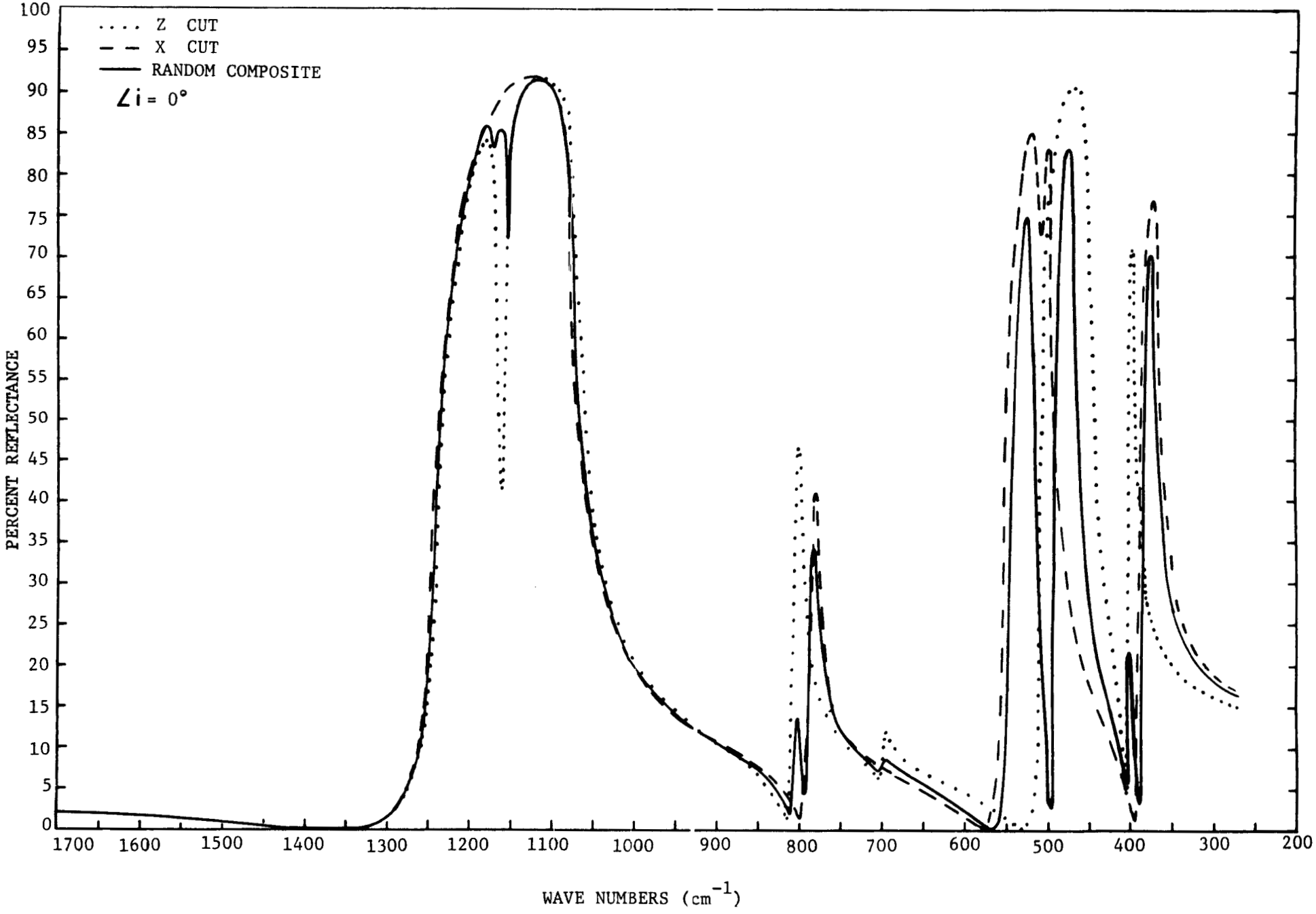

FIGURE 22. CALCULATED REFLECTANCE SPECTRA FOR ORIENTED QUARTZ AND RANDOM COMPOSITE

shifting is apparent due to the way in which the slopes of the individual curves interact. The 500 cm^{-1} feature in X-cut quartz has been reduced to a shoulder which is slightly shifted in frequency in the mixture and is apparently replaced by a valley at 500 cm^{-1}.

In Figure 23, we have plotted the effect of vacuum packing fraction on the spectrum using a log scale. The top curve is our 2:1 mix with no vacuum or air space (i.e., $f_Z + f_X = 1$). The middle curve has the same quartz mix but $f_Z + f_X = 0.5$ and $f_{vac.} = 0.5$. The lowest curve continues the series to $f_{vac.} = 0.9$. It is quite clear from the figure that according to this quantitative mixing rule the spectral features remain even at low packing fractions, which agrees with our previously reported[17,18,25] conclusions concerning spectral contrast (see Table II). The mixing rule used here is general in contradistinction to the special case rules used before,[17,18,25] (equations 16 and 17), which resulted in the simple relationship of packing fraction to reflectance (equation 5). Figure 23 takes into account the effect of changes in the refractive index due to anomalous dispersion and is therefore a further improvement on Table II.

Because of the difficulty of application of such a complex mixing rule in disentangling the spectra of mixtures (one needs to know the optical constants rather than simply the emittance or reflectance spectrum), a comparison with the spectrum expected from a simple mixing rule such as that used for large grains is shown in Figure 24. While the spectra are similar in most places, important discrepancies can be seen near 1160 cm^{-1} and 500 cm^{-1}.

We invoke the results of Figure 13 in order to verify the validity of our mixing rule experimentally. These results appear to confirm the general validity of the complex mixing rule as well as the effect of packing fraction. Some discrepancies between our experimental and theoretical values can be accounted for by the experimental spectral slit widths used and the variation between the calculated reflectance at

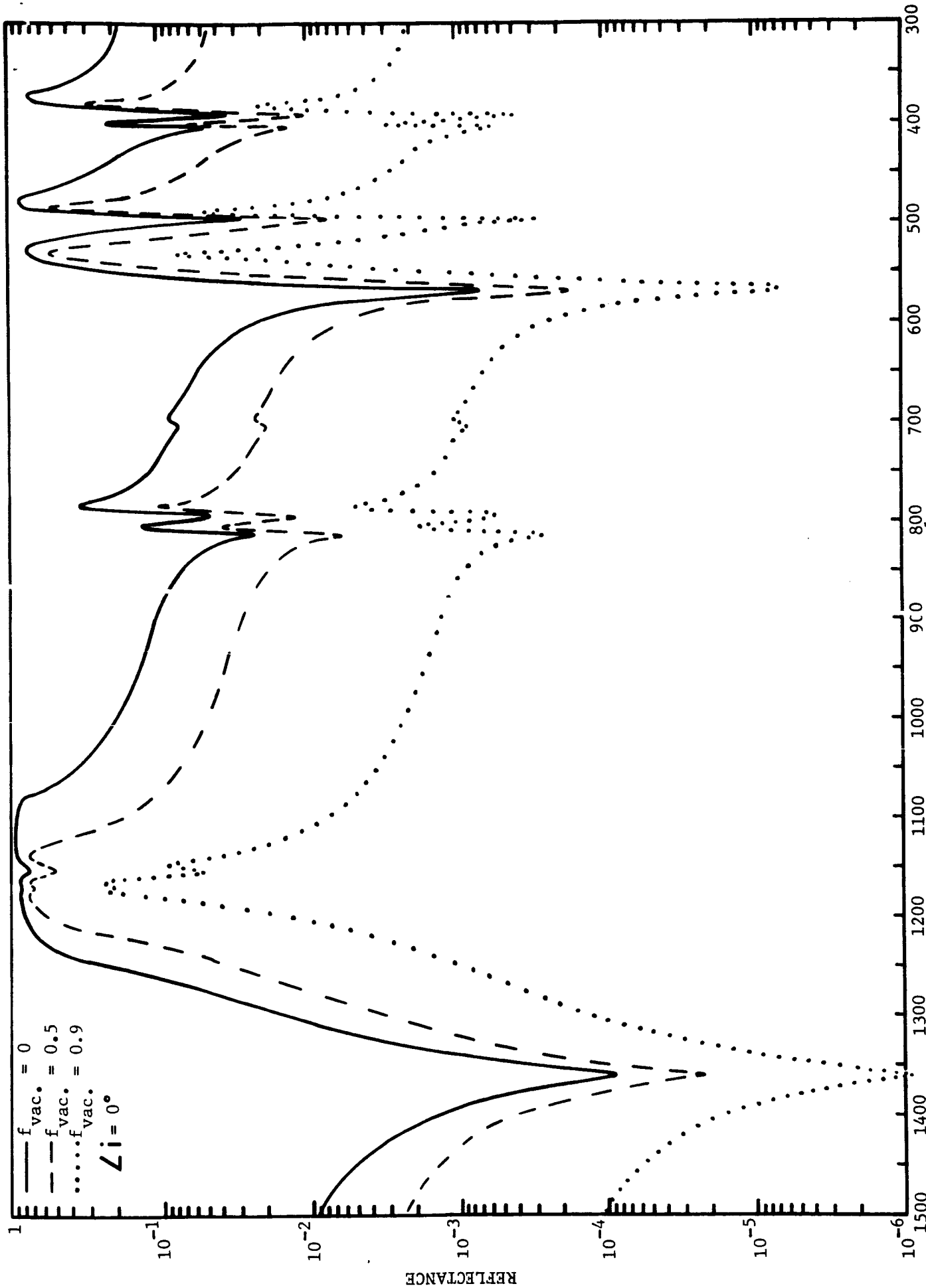

FIGURE 23. CALCULATED REFLECTANCE SPECTRA OF RANDOM QUARTZ FOR DIFFERENT VOLUME FRACTIONS

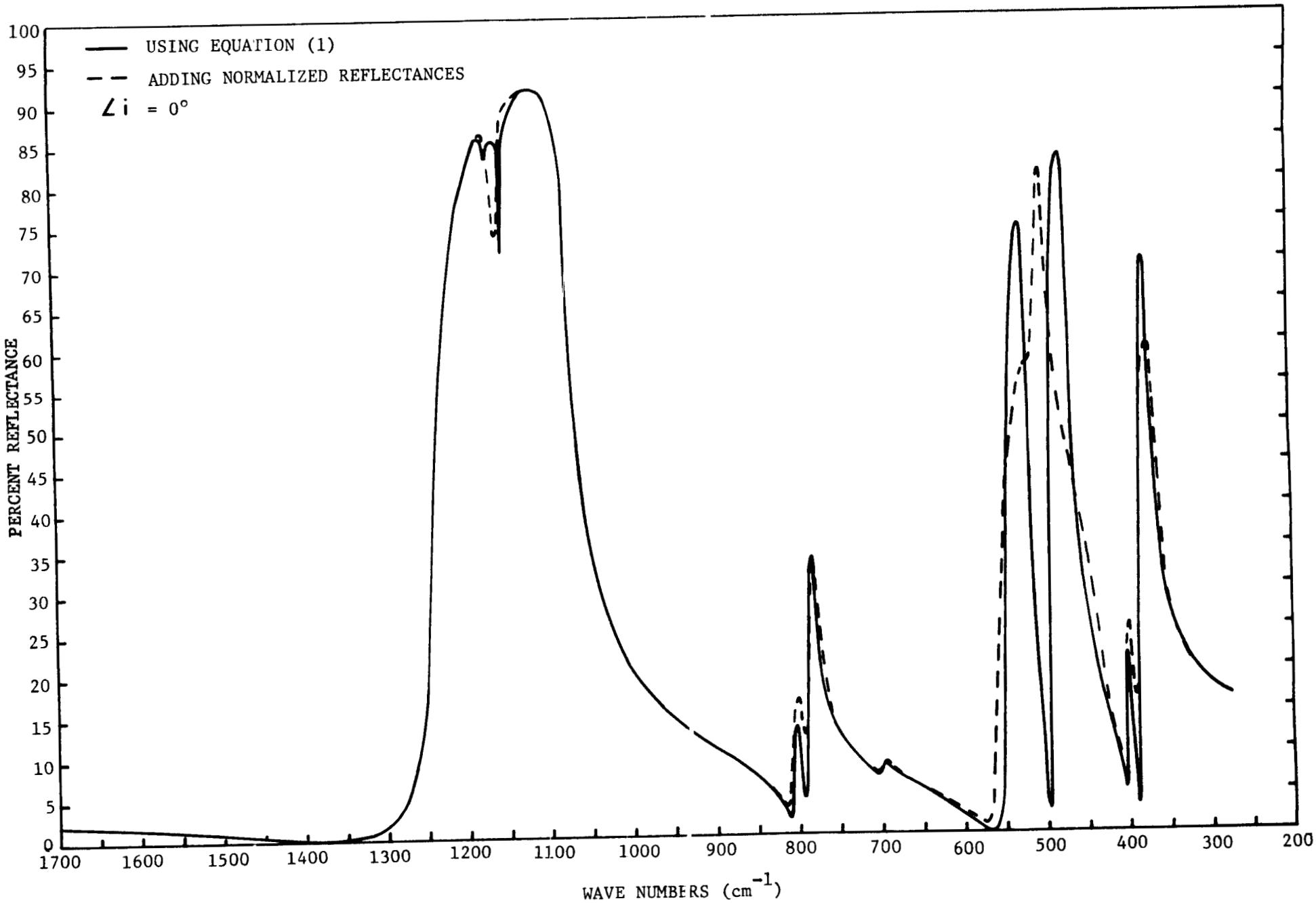

FIGURE 24. CALCULATED COMPOSITE REFLECTANCE SPECTRA USING DIFFERENT MIXING RULES

normal incidence and the measured reflectance at 45°. In addition, our Golay cell was discovered to be in the process of breaking down shortly after these spectra were run. Therefore, we rechecked our experimental data for the upper curve and found a deviation of about 1% from the data shown.

The experimental shape in the middle infrared region near 9 microns appears to deviate from either the simple or complex mixing rule (see insert in Figure 20), though retaining apparent features of both. This is not too surprising as the wavelength at this point is not very far removed from the particle size, and some more complex rule is probably necessary. As stated before, we feel additional effort is required here.

B. DERIVATION OF THE GENERAL MIXING RULE FOR FINE POWDERS

The reflectance of a medium composed of a mixture of fine particles (small compared with the wavelength) and vacuum depends on the macroscopic optical constants n and k of the medium. Scattering is negligible compared with the coherent surface reflection if the particles are very small compared with the wavelength and sufficiently densely packed so that n - 1 and k differ appreciably from zero.

The complex index of refraction n - ik is related to the complex dielectric constant ϵ of the composite medium by the relation

$$\epsilon = (n - ik)^2 \qquad (22)$$

Thus the problem of deriving a mixing rule for n - ik is equivalent to that of obtaining a mixing rule for ϵ. Now Clausius and Mossotti long ago proposed an explanation of the dielectric constant of materials in terms of the polarization of an assembly of conducting spheres. Lorentz and Lorenz improved on this model by attributing the polarization of the

medium to the polarization of the individual molecules of the medium. We shall carry the argument one step further by applying the same idea to an assembly of spherical polarizable particles of dimensions that are macroscopic but still small compared with the wavelength of the radiation.

The Lorentz-Lorenz theory is based on the idea that the polarization of an individual molecule is due to the sum of the externally applied electric field E and the field E_i caused by the induced electric dipole moments of all the other molecules.

Let α be the polarizability of a molecule. Then the induced dipole moment is, by definition,

$$\mu = \alpha (E + E_i) \tag{23}$$

If there are N molecules per unit volume, the polarization of the medium is

$$P = N\mu \tag{24}$$

The theory now assumes that the individual molecule under consideration is effectively located at the center of a spherical cavity in a homogeneous medium composed of a smoothed-out distribution of all the other molecules. Then the internal field is, by a well-known result of electrostatics,

$$E_i = \frac{4 \pi P}{3} \tag{25}$$

The dielectric constant of the medium is

$$E = 1 + 4 \pi \frac{P}{E} \tag{26}$$

On combining equations 23-26, one gets the Lorentz-Lorenz relation

$$\frac{\epsilon - 1}{\epsilon + 2} = \frac{4 \pi N\alpha}{3} \tag{27}$$

In our extension of the theory to a fine mixed powder we do two things. First we replace $N\alpha$ by the appropriate expression for a mixture of particles of different N's and α's. Second we express the α's in terms of the dielectric constants of the bulk materials of which the particles are composed. Thus for the mixed powder

$$\frac{\epsilon - 1}{\epsilon + 2} = \frac{4 \pi}{3} \sum_p N_p \alpha_p \tag{28}$$

$$\alpha_p = \frac{\epsilon_p - 1}{\epsilon_p + 2} a_p^3 \tag{29}$$

where N_p, α_p, ϵ_p, a_p are, respectively, the number of particles per unit volume, the polarizability, the dielectric constant, and the radius of particles of type p. Equation 29 is another well-known result of electrostatics for the polarizability of a dielectric sphere.

On substituting (29) into (28) and noting that $4 \pi a_p^3 N_p/3$ is the fraction f_p of the volume occupied by type-p particles, we arrive at the mixing rule for dielectric constants

$$\frac{\epsilon - 1}{\epsilon + 2} = \sum_p f_p \cdot \frac{\epsilon_p - 1}{\epsilon_p + 2} \tag{30}$$

The mixing rule for the optical constants can now be written down with the help of equation (22) to give

$$\frac{(n - ik)^2 - 1}{(n - ik)^2 + 2} = \Sigma_p f_p \frac{(n_p - ik_p)^2 - 1}{(n_p - ik_p)^2 + 2} \qquad (21)$$

The volume fractions f_p do not add up to unity since in general there are empty spaces between the particles. However, since $n_p - ik = 1$, for vacuum, the summation can formally include a term to represent the vacuum. Under these conditions the sum of the f_p's will be unity.

Note added in proof

A private communication received from Dr. John Wood of the Smithsonian Astrophysical Observatory, while this report was being processed, has slightly revised his original estimate of the composition of the Forest City Chondrite.[1] The pyroxenes present are better represented by 24.5 wt% for the orthorhombic form and 2.2 wt% for the monoclinic form which is probably diopside. Our composite calculations shown in Figure 21 are essentially unchanged by the new information.

V. REMOTE SENSING CONSIDERATIONS

During the course of this program, Arthur D. Little, Inc., submitted a proposal to the National Aeronautics and Space Administration, Washington, D. C., entitled "Mapping of the Composition of the Surface and Atmosphere of Mars by an Orbiting Broadband Infrared Interferometer."[2] This proposal summarizes our thinking as to the kind of experiment that should be put on the Voyager Mission but could be readily adapted to a lunar orbiter mission. In essense, we feel that an orbiting broadband infrared interferometer is capable of ascertaining the chemical composition of the lunar surface and its state of aggregation. The Martian Voyager experiment was designed without cooled detectors due to their high power and weight requirements necessary on such a long mission. There are other differences between Martian and Lunar missions such as the need to look through the Martian atmosphere, and a search for the possible presence of organic species on Mars. Basically, however, we feel that a broadband interferometer (approximate range 2.5 to 85 microns) having 10 cm^{-1} resolution would be the best instrument that could be placed on a lunar orbiter to measure the composition of the lunar surface. We later modified this instrument slightly to satisfy the constraints of a Martian Mariner flyby mission.

A typical set of specifications for such an instrument without cooling are

Wavelength range	2.5-85 microns
Spectral resolution	10 cm^{-1}
Half angle of viewing cone	4 degrees
Aperture	9 cm^2 (for each section of this 3-channel instrument)
Scan time	2.5 seconds
Noise equivalent spectral radiance (NESR)	betweem 2×10^{-9} and 1.8×10^{-8} watt/cm^2 steradian cm^{-1}

A graph of the expected signal-to-noise ratio of the spectrum (as derived from one interferogram) with wavelength and frequency is shown in Figure 25a.

The calculated signal-to-noise ratio is based on certain assumptions (e.g., a gray body with an emittance of 0.9). For our purposes a more important quantity is the ratio of the change in signal, that arises from a change in emittance or reflectance, to the noise. Therefore, performance is better judged by the plot shown in Figure 25b of "Noise equivalent reflectance increment" vs frequency. The total radiance, J of Mars for instance, consists of reflected solar and emitted thermal radiation.

$$J_{Mars} = R\, J_{solar} + (1 - R) J_{thermal} \tag{31}$$

Differentiation with respect to R, equating the resulting ΔJ to the noise equivalent spectral radiance and taking absolute values, yields

$$|\Delta R| = \frac{NESR}{|J_{solar} - J_{thermal}|} \tag{32}$$

which is shown in Figure 25b and is the smallest detectable feature for the suggested instrument. It should be noted that improvements in the instrument could be made by the use of cooled detectors and coherent addition of individual interferograms. The viewing cone angle together with the instrumental altitude, scan time, and instrumental velocity set the areal resolution obtainable. For the Voyager Mission we calculated an areal resolution of the order of 100 km.

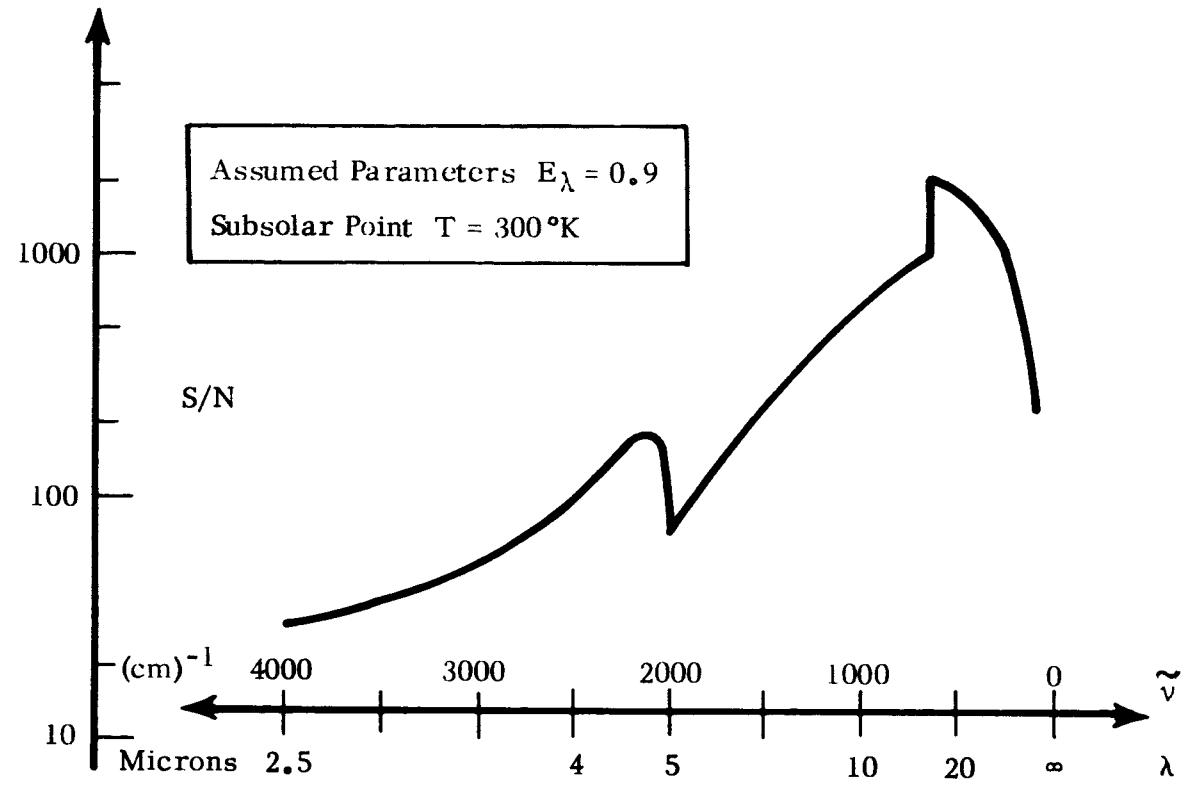

a. SIGNAL TO NOISE RATIO

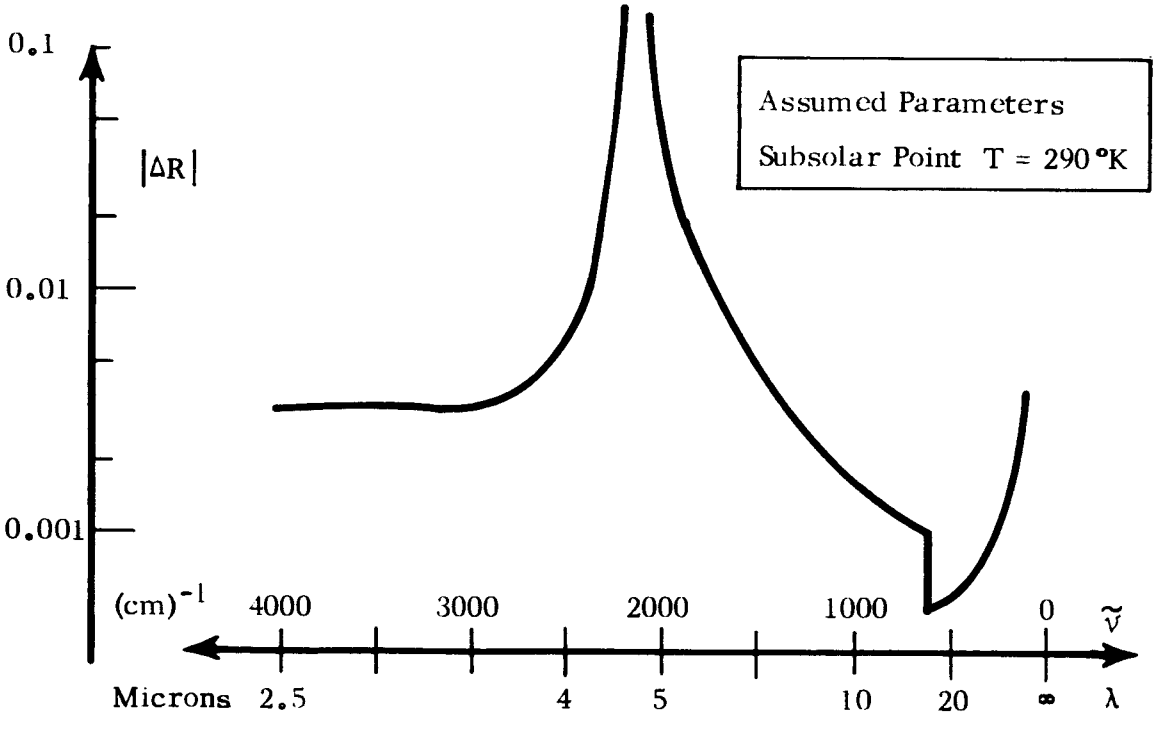

b. NOISE EQUIVALENT REFLECTANCE INCREMENT

FIGURE 25. EXPECTED INTERFEROMETER PERFORMANCE

VI. SUGGESTIONS FOR FURTHER WORK

A number of topics require additional effort in order to fully understand the phenomena and utilize the data in remote sensing applications. They include:

(1) continued measurements of the far-infrared spectra of possible lunar and planetary surface minerals in bulk form to serve as the nucleus of a catalogue of mineral spectra in the far-infrared region to supplement existing middle-infrared data. This work could be accelerated by the used of a broadband-infrared interferometer. Such instruments are commercially available.

(2) the further study of the effects of surface roughness on spectral shape and intensity for the case of samples composed of fine particles (and therefore having diluted optical constants). This should be done for gently undulating surfaces like those already investigated, for surfaces similar to the wind-packed surfaces that may well exist on Mars, and for pumice-like surfaces and surfaces obtained by sifting the powder in a vacuum to represent possible lunar conditions.

(3) further verification of the mixing rules we have derived for composite samples, their modification for particle sizes near the wavelength and derivation of simplified approximate rules for use in spectral stripping techniques.

(4) development of a computer program for spectral stripping, probably based on cross-correlation techniques with a library of individual spectra.

(5) experimental determination of the relationship between the normal emittance and single-angle reflectance of a variety of bulk and particulate mineral samples.

VII. REFERENCES

1 J. R. Aronson, H. G. McLinden, and R. V. Allen, Final Report, Part II, Contract NAS8-2537 to George C. Marshall Space Flight Center, NASA (1965).

2 Arthur D. Little, Inc., Technical Proposal to NASA, Washington, D.C. "Mapping of the Composition of the Surface and Atmosphere of Mars by an Orbiting Broadband-Infrared Interferometer," November 15, 1965.

3 R. J. P. Lyon, Minerals in the Infrared, Stanford Research Institute (1962).

4 R. J. P. Lyon, "Evaluation of Infrared Spectrophotometry for Compositional Analysis of Lunar and Planetary Soils," NASA TN D-1871 (1963).

5 R. J. P. Lyon, Stanford Research Institute Final Report, Part II, Contract NASr-49(04) (1964); NASA CR 100 (1965); Econ. Geol. 60, 715 (1965).

6 R. C. Lord and T. K. McCubbin, Jr., J. Opt. Soc. Am. 47, 689 (1957).

7 J. R. Aronson and H. G. McLinden, "An Investigation of the Optical Properties of Materials at Room and Liquid Helium Temperatures," Final Report, Contract NAS8-2537 to George C. Marshall Space Flight Center, NASA, November 30, 1963.

8 E. D. Palik, N. R. L. Bibliography, No. 21, U. S. Naval Research Laboratory, April 1963.

9 L. E. S. Mathias and A. Crocker, Phys. Letters 13, 35 (1964).

10 P. Tarte, Spectrochim, Acta 18, 467 (1962); ibid 19, 25 (1963); ibid 19, 48 (1963).

11 P. Tarte, Bull. Soc. franc. Ceram. 58, 13 (1963).

12 G. R. Hunt and J. W. Salisbury, Science 146, 641 (1964).

13 W. A. Hovis, Jr., Icarus 4, 425 (1965); Appl. Opt. 5, 245 (1966).

14 R. Van Tassel and I. Simon, "Thermal Emission Characteristics of Mineral Dusts" in The Lunar Surface Layer, Eds. Salisbury and Glaser, Academic Press, New York (1964).

15 W. Corliss, Space Probes and Planetary Exploration, Van Nostrand Co., 1965, p. 434.

16 H. C. Van de Hulst, Light Scattering by Small Particles, John Wiley & Sons, In.c, New York 1957.

17 J. R. Aronson, A. G. Emslie, and H. G. McLinden, "Infrared Spectra from Fine Particulate Surfaces," Science 152, 345 (1966).

18 A. G. Emslie, AIAA Paper No. 65-667, to be published in Progress in Astronautics and Aeronautics.

19 W. R. Blevin and W. J. Brown, J. Opt. Soc. Am. 51, 129 (1961).

20 A. Schuster, Astrophys. J. 21, 1 (1905).

21 H. H. Blau, Jr., and R. P. Espinola, Arthur D. Little, Inc., Final Report, Contract Non-3556(00), June 1965.

22 K. Keil and K. Fredriksson, J. Geophys. Res. 69, 3487 (1964).

23 G. Kunz, Amer. J. Sci. 40, 320 (1890).

24 W. G. Spitzer and D.A. Kleinman, Phys. Rev. 121, 1324 (1961).

25 J. R. Aronson and H.G. McLinden, AIAA Paper No. 65-668, to be published in Progress in Astronautics and Aeronautics.